Computers and Electronics in Agriculture 212 (2023) 108124

Contents lists available at ScienceDirect

Computers and Electronics in Agriculture

journal homepage: www.elsevier.com/locate/compag

Coupled maize model: A 4D maize growth model based on growing degree days

Binxiang Qian [a,b], Wenjiang Huang [a,b,c,*], Donghui Xie [d], Huichun Ye [a,b,c], Anting Guo [a,b,c,*], Yuhao Pan [a,b], Yin Jin [a,b], Qiaoyun Xie [e], Quanjun Jiao [a,b], Biyao Zhang [a], Chao Ruan [f], Tianjun Xu [g], Yong Zhang [g], Tiange Nie [g]

[a] Key Laboratory of Digital Earth Science, Aerospace Information Research Institute, Chinese Academy of Sciences, Beijing 100094, China
[b] International Research Center of Big Data for Sustainable Development Goals, Beijing 100094, China (*University of Chinese Academy of Sciences, Beijing 100049, China
[c] Key Laboratory of Earth Observation of Hainan, Aerospace Information Research Institute, Chinese Academy of Sciences, Sanya 572029, China
[d] The State Key Laboratory of Remote Sensing Science, Institute of Remote Sensing Science and Engineering, Faculty of Geographical Science, Beijing Normal University, Beijing 100875, China
[e] School of Engineering, The University of Western Australia, Perth, WA 6009, Australia
[f] National Engineering Research Center for Agro-Ecological Big Data Analysis and Application, Anhui University, Hefei, China
[g] Maize Research Institute of Beijing Academy of Agriculture and Forestry Sciences, Beijing, China

ARTICLE INFO

Keywords:
Remote sensing
Maize growth model
4D maize growth model
Maize canopy parameters
Growing degree days (GDDs)
Coupled maize model

ABSTRACT

Crop canopy parameters are critical for environmental remote sensing, describing crop phenotypes, and ensuring food security. Evaluating the effect of temperature on crop growth is crucial for estimating crop canopy parameters. However, existing crop growth and plant functional-structural models cannot simultaneously model temperature responses, perform accurate dynamic simulations, and provide multi-scale computer visualizations. This limitation has hindered the application of structural models of maize plants for use in 3D radiative transfer models, crop structure evaluations, and crop phenotype descriptions. We improve the leaf/organ-level thermal-driven crop growth model (MAIZSIM) and the plant functional-structural algorithm. To address these limitations, we propose the coupled maize model, a four-dimensional (4D) growth model based on growing degree days. This model can simulate and visualize the structural parameters of the maize canopy at the organ, plant, seasonal, and population levels. The model outputs three-dimensional (3D) predictions of the maize structure (file format.obj), enabling editing and 3D visualizations. We use maize datasets from multiple phenological periods to test the proposed model's accuracy and stability in simulating the canopy parameters at multiple levels. The results show that the normalized root mean square errors (NRMSEs) between the simulated and measured maize leaf size, area, leaf node height, and vein curve derived from the coupled maize model are below 0.1, demonstrating the model's high accuracy.

1. Introduction

Crop canopy parameters are required for environmental remote sensing and climate change studies and for describing crop phenotypes. They provide essential information for crop growth monitoring, yield prediction, and production management decisions(Li et al., 2022). Crop canopy parameters encompass both biophysical parameters (such as plant architecture, leaf area index, leaf angle distribution, etc.) and biochemical parameters (including chlorophyll content, nitrogen content, etc.). In this study, our focus is on the biophysical parameters specifically related to the three-dimensional distribution of crop canopy structure, namely the three-dimensional structural parameters of the crop canopy. An ideal crop growth model can accurately describe changes in the canopy parameters, biomass accumulation, and nutrient transfer at multiple scales during the growth period, including the organ, plant, seasonal, and population levels(de Reffye et al., 2020; Kim et al., 2012). This accuracy is critical for the real-time prediction, monitoring, and evaluation of crop growth and development(Gao et al.,

* Corresponding authors at: Key Laboratory of Digital Earth Science, Aerospace Information Research Institute, Chinese Academy of Sciences, Beijing 100094, China.
E-mail addresses: huangwj@aircas.ac.cn (W. Huang), guoat@aircas.ac.cn (A. Guo).

https://doi.org/10.1016/j.compag.2023.108124
Received 4 April 2023; Received in revised form 24 June 2023; Accepted 30 July 2023
Available online 11 August 2023
0168-1699/© 2023 Elsevier B.V. All rights reserved.

2017; Wang et al., 2018). However, conventional crop growth models often solely simulate abstract (statistical) canopy traits, such as leaf area index, while failing to capture the intricate three-dimensional structural information of plant canopies, including leaf angle distribution, leaf shape, and leaf curvature. To overcome this limitation, the integration of plant phenomics becomes imperative. Plant phenotypic traits are classified into morphological, physiological functional, and component traits(Tardieu et al., 2017). High-throughput, high-precision, and multi-dimensional phenotypic data acquisition and analysis technologies are promoting the rapid development of genetic improvement in plant breeding and advances in precision agriculture(Li et al., 2020; Tao et al., 2022). Plant functional-structural models, informed by prior knowledge from plant phenomics, facilitate the conversion of statistically modeled crop canopy parameters derived from the crop growth model into three-dimensional structural information of plant canopies, which can be further visualized using computer-based techniques.

To accurately simulate and reconstruct the three-dimensional structural parameters of crop canopies that undergo changes throughout the growth stages, the establishment of precise crop growth models is imperative. The accurate characterization of plant response to temperature is required to establish and implement accurate crop growth models(Yan and Hunt, 1999). Numerous crop growth models based on plant responses to temperature (thermodynamics), water, and fertilizer have been widely used to estimate crop canopy parameters. We divided crop growth models into three categories according to the model type: individual or group level, leaf or organ level, and enzyme or cellular level models. Although individual or group-level models, which are the most common ones, can estimate the statistical parameters of the canopy structural characteristics, phenology, biomass accumulation, and yield accurately, they do not provide sufficient descriptions of the crop's leaf structure. Significant progress has been made in recent years in developing crop growth models at the leaf or organ level. MAIZe SIMulation (MAIZSIM) is one of the most representative crop growth models at the leaf or organ level, using a function to calculate temperature-dependent processes (R(T)) to estimate leaf growth rates precisely under different temperatures(Kim et al., 2012). Additionally, this model can be used to study crucial physiological and physical processes in maize, such as C4 photosynthesis, canopy radiation transfer, carbon allocation, water relations, and nitrogen dynamics.

Plant phenomics plays a crucial role in converting statistically modeled crop canopy parameters from crop growth models into three-dimensional structural information of plant canopies at various scales, thereby facilitating computer-based three-dimensional reconstruction. With the rapid advancement of diverse imaging techniques and phenotyping platforms, substantial strides have been achieved in the phenotyping of plant organ phenotypes, whole-plant phenotypes, and 3D plant phenotypes(Li et al., 2020; Tao et al., 2022). However, algorithm and software advances and plant functional-structural models have provided excellent results, such as L-system–based simulators (L-studio) (Allen et al., 2005), A software suite for Plants Architecture Modelling (AMAP-studio)(Griffon and De Coligny, 2014), Functional-Structural Plant Models (FSPM)(Vos et al., 2010), GroImp Modeling Platform (GroIMP)(Hemmerling et al., 2013), and others. These models can simulate the 3D morphology of maize accurately. In addition, AMAP-studio and GroIMP allow for editing the 3D morphology of maize plants and describing the dynamic changes in individual plants during growth. However, the lack of information on accurate maize physiology limits the ability to model the crop's responses to environmental stress and simulate the dynamic changes in maize's 3D morphology accurately.

In this study, we have innovatively coupled the crop growth model with the plant functional-structural model. This coupling leverages the advantages of the plant functional-structural model in providing multi-scale and three-dimensional visualization of crop canopy structure parameters. It aims to compensate for the limitation of the crop growth model, which can only simulate abstract canopy structural characteristics. The objective of this study is to analyze the structural parameters of the aboveground non-reproductive organs of maize, such as the stems and leaves, during growth and development, i.e., from emergence to tasselling. We evaluate the temperature response of maize using the thermal-driven crop growth model (MAIZSIM) at the leaf or organ level, specifically the effect of $GDD_{8°C}$ (growing degree days with 8 °C as the lowest threshold temperature) on the canopy structure. A 3D Functional-structural plant models (España et al., 1999) is improved, and a four-dimensional (4D) model (3D plus time) is established to reconstruct the maize canopy parameters and evaluate the effect of GDD on the plant response. We refer to this model as the coupled maize model. We use a multi-growing season maize dataset to validate the accuracy and stability of the coupled maize model for simulating the canopy parameters at the organ, individual, season, and population levels.

2. Materials and methods

2.1. Data overview

The field experiment aimed to study the growth and development of summer maize. It was conducted at the Tongzhou Experimental Station of the Beijing Academy of Agriculture and Forestry Sciences in Beijing, China (116°41.7′E, 39°41.1′N). The experimental field was situated in a warm, semi-humid continental monsoon climate zone with a mean annual precipitation of 620 mm and an average annual temperature of 13.3 °C. The soil type of the experimental field was brown soil. The experiment was conducted in 2022, and the experimental area was divided into six test plots (10 m × 30 m), and the maize variety is MC121. In the experimental field, the average inter-row spacing of maize plants (d_{row}) was 60 cm, the average intra-row spacing (d_{col}) was 25 cm, and the population density was estimated to be approximately 66,000 $plants{\cdot}ha^{-1}$. The maize was sown every 10 days (May 1, May 10, May 20, May 31, June 10, and June 20). At each planting location, two maize seeds were sown, and at the four-leaf stage, one plant exhibiting growth characteristics that closely matched the overall condition of the experimental plot was selected for retention, while the other plant was manually removed. Furthermore, in rare cases where both seeds failed to germinate, transplantation was conducted at those specific locations. On July 21, canopy parameter data were collected, and the GDD at a temperature of 8 °C ($GDD_{8°C}$) of the six plots were 580, 680, 739, 904, 995, and 1192 $day{\bullet}°C$, respectively. We selected five sample plots (1 m × 1 m) on the diagonal in each test plot and measured the canopy parameters, including the average stem height, stem diameter, number of leaves, average leaf node height, average length, width, area, shape, and vein curvature angle of each leaf, LAI, whole plant dry and wet weight, leaf pigment, and nitrogen content. In the measurement of three-dimensional structural parameters of the maize canopy, leaf shape and leaf curvature pose the greatest measurement challenges. To measure leaf shape, we carefully flattened each leaf on the floor and divided it into 10 equally sized segments. Following the diagram depicted in Fig. 2b, we accurately measured the width of each leaf segment and employed a quadratic function to formulate the leaf shape equation. When measuring leaf curvature, we captured frontal photographs of the maize plants and employed digital image analysis techniques, following the diagram depicted in Fig. 2a, to quantify the vein curvature angle of each leaf. Meteorological data were obtained from the TYD-ZS1 agricultural meteorological monitoring system, which was installed on a fixed bracket at the height of 3 m. The system measured environmental temperature, humidity, soil temperature, humidity, wind direction, wind speed, and rainfall every 10 min. The hourly average temperature was used to assess maize growth and development. Table 1 presents the details of the datasets.

Table 1
The measured and predicted values of the maize parameters.

	Name*	Size	Average value of maize canopy parameters					
			Leaf length (cm)	Leaf width (cm)	Leaf aspect ratio	Leaf area (cm^2)	Leaf height (cm)	Leaf curvature (°)
Measured values	M_{580}	40	66.9	8.5	0.130	350.9	41.5	40.8
	M_{680}	48	77.7	8.7	0.114	382.6	85.6	55.1
	M_{739}	52	73.6	8.9	0.135	379.4	88.5	52.2
	M_{904}	56	79.1	8.7	0.111	394.5	126.5	56.1
	M_{995}	56	76.7	8.7	0.116	423.7	129.9	53.2
	M_{1192}	56	79.4	8.8	0.112	446.7	13.1	53.9
Predicted values	P_{580}	10	66.4	7.9	0.119	336.3	43.5	40.8
	P_{680}	12	73.0	8.7	0.119	378.1	86.5	51.4
	P_{739}	13	71.0	8.4	0.119	364.2	88.8	53.3
	P_{904}	14	78.0	9.3	0.119	420.6	125.4	56.9
	P_{995}	14	75.3	9.0	0.119	436.3	133.4	48.9
	P_{1192}	14	80.2	9.0	0.119	459.0	134.1	55.3

* M580 and P580 represent experimental measurement data sets and model simulation data sets for maize canopy parameters at GDD_(8 °C) = 580 day•°C, respectively.

2.2. Coupled maize model algorithm

2.2.1. Mathematical description of maize plant at the organ level

Maize plants consist of roots, stems, leaves, ears, and grains. This study focuses on the mathematical description of two non-reproductive organs: stems and leaves. The phenotype of maize stems and leaves is influenced by internal factors, e.g., gene type, and external factors, such as climate, water, and fertilizer stress. We only consider ideal conditions and conduct a mathematical description of the growing season to analyze the effect of $GDD_{8°C}$ on the maize stem phenotype. The structural parameters at the organ level include the i^{th} leaf's order, length, width, shape, and curvature and the i^{th} segment of the stem's bottom and top diameters, and the height.

1) Mathematical description and computer visualization of the maize stem.

At the organ level, maize stems are comprised of multiple stacked frustums of a cone. Regular hexagonal prisms can be utilized to simplify the frustums and facilitate computer visualizations of 3D maize models. In this case, the stem top and bottom diameters of the i^{th} stem segment are defined by the diameter of the circumcircle of the upper and lower bases of the regular hexagonal prism, respectively. Correspondingly, the length of the i^{th} stem segment is represented by the height of the regular hexagonal prism. When the stem top and bottom diameters are similar, a regular hexagonal prism is used to replace the frustum pyramid. Fig. 1 illustrates the geometric simplification of a maize stem into multiple stacked regular hexagonal prisms. Each was divided into 12 triangular meshes for computer visualization (Fig. 1 **e**).

2) Mathematical description and computer visualization of the maize leaf.

The mathematical description of the maize leaf is more complex than that of the maize stem. The structural parameters of maize at the leaf level include the leaf order, leaf size, leaf shape, leaf curvature, and leaf azimuth.

(a) The leaf order refers to the sequence of leaf growth and development, i.e., the order in which leaves appear from the ground to the top of the stem. The leaf order of the closest leaf to the ground is denoted as 1, and that of the highest leaf is denoted as N_t.
(b) The leaf size is determined by the maximum length and width of the leaf. **Equation (1)** describes the proportional relationship between the maximum length $l_{max\,i}$ and maximum width $w_{max\,i}$ of leaf *i*. The leaf aspect ratio, an empirical coefficient, is defined as the ratio of $l_{max\,i}$ and $w_{max\,i}$. A value of 0.106 was used in previous studies(Kim et al., 2012; Lizaso et al., 2003). In our study, we used a leaf aspect ratio of 0.119. The leaf size of leaf *i* ($l_{max\,i}$ and $w_{max\,i}$) depends on the leaf order *i* for determining the genotype. More detailed mathematical equations have been developed to describe maize plants at the leaf level.

$$w_{max\,i} = l_{max\,i} * LeafAspectRatio \quad (1)$$

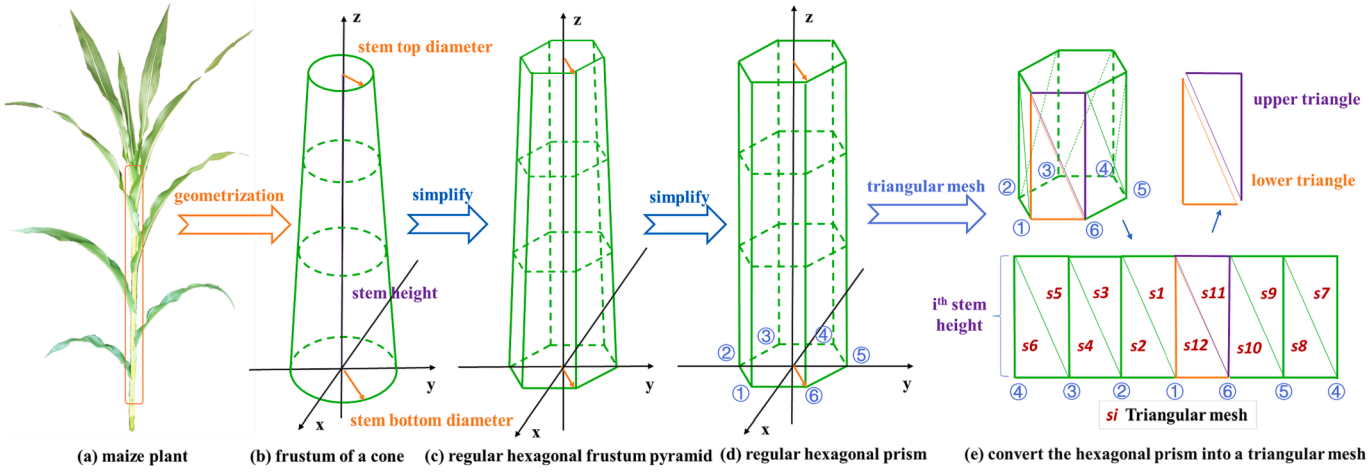


Fig. 1. Mathematical description and computer visualization of the maize stem.

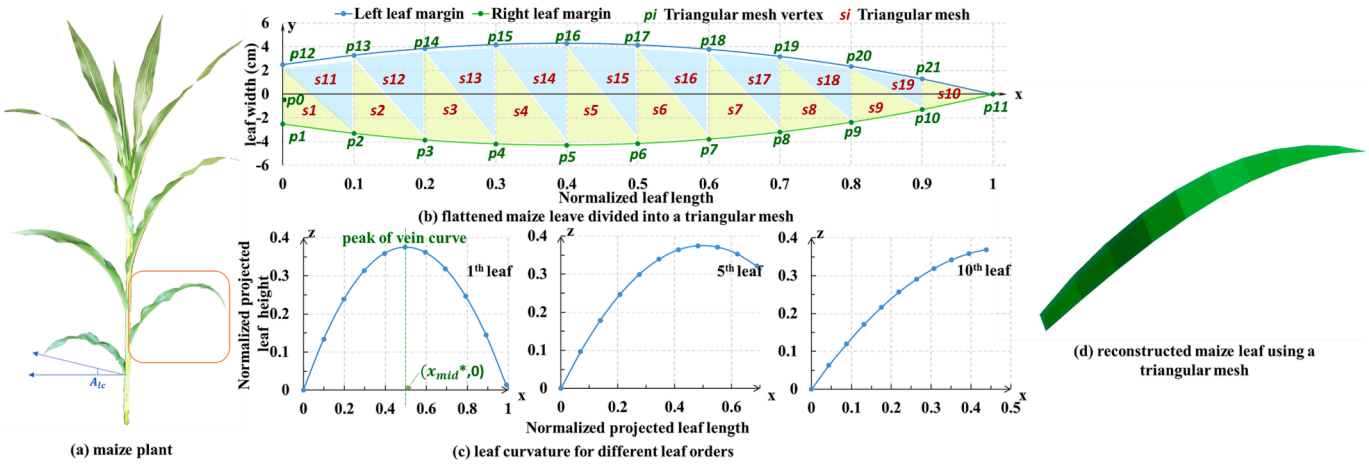


Fig. 2. Mathematical description and computer visualization of the maize leaf.

(c) Leaf shape. We consider the leaf shape when it is spread out on the x-y plane. It is described by the length and width of the leaf, and the width is variable from the leaf sheath to the leaf tip. Several key concepts are defined to describe the leaf shape mathematically, including the leaf veins, the length and width of leaf segments, and the normalized length of leaf segments(Wu et al., 2002). The leaf vein is the central axis of symmetry when a maize leaf is spread out, and the distance from any point on the leaf vein to the stem leaf node ***P0*** is referred to as the length of the leaf segment (***l***). The normalized length of the leaf segment is expressed by l^* in **Eq. (2)**. The width of the leaf segment (***w***) is defined as the distance between the intersection points of a line perpendicular to the leaf vein passing through any point on the leaf vein and the edge of the leaf. This concept is depicted in Fig. 2 **b**.

$$l^* = l/l_{max} \tag{2}$$

where l_{max} represents the maximum length of the leaf blade.

Maize leaves exhibit significant variations in shape at different heights. Therefore, we divide the leaves into the bottom, middle, and upper leaves. The bottom leaves are short and slender, the middle leaves are long and wide, and the upper leaves have a wide base and rapidly taper towards the tip(Wu et al., 2002). We establish a quadratic equation (**Eq. (3)**) to describe the relationship between the width of a leaf segment (w) and its normalized length (l^*) (España et al., 1999). As shown in Fig. 2 **b**, the leaf blade is segmented into ten equal parts using eleven points (*P1* to *P11*). When $l^* = 1$, the equation describes the width of the leaf blade at the tip, where $w = 0$, and $\alpha = -(\beta + \gamma)$. When$l^* = 0$, the equation describes the width of the leaf blade at the sheath, where $w = \gamma^* l_{max}$. Each leaf is partitioned into 19 triangular meshes (S_1-S_{19}) using twenty-one points (*P1-P21*) for computer visualization.

$$w = (\alpha^* {l^*}^2 + \beta^* l^* + \gamma)^* l_{max} \tag{3}$$

where l_{max} denotes the maximum length of leaf blade i, and α, β, and γ represent empirical coefficients. These coefficients depend on the leaf node height (bottom, middle, or upper leaves), the leaf aspect ratio, and the maximum number of leaves (N_t). For instance, when the leaf aspect ratio is 0.119, and N_t is 20, the empirical coefficients of the leaf shape equation are $\alpha = 0.2788$, $\beta = 0.2288$, and $\gamma = 0.05$. We ignored the wave-like movements of the leaves to reduce model complexity and the number of triangular meshes and enhance visualization efficiency. A comprehensive study of this feature has been conducted by España and Baret(España et al., 1999).

(d) Leaf curvature. The natural bending of the leaf veins, known as leaf curvature, is influenced by genetic traits, climate, and mechanical mechanisms. We assume that the leaf veins are positioned in the same vertical plane and project them onto the x-z plane, as depicted in Fig. 2**c**. To replicate the curvature of maize leaf veins, we establish a quadratic function *lc*, which is analogous to the normalized dimensionless number used to describe leaf shape. The leaf vein curvature projected onto the x-axis is referred to as x*, and the height of the curvature projected onto the z-axis is denoted as z*. The vertex of the leaf vein curvature is identified as the point with the highest z* value, while the distance from the projection of the vertex on the x-axis to the stem and leaf junction (0,0) is denoted as x_{mid}, representing the half-width of the leaf vein curvature. We then normalize the points (x, z) on the leaf vein curvature using **Eqs. (4) and (5)** to express the leaf vein curvature using **Eqs. (6)**, **7**, and **8**. The curvature of maize leaves depends on the leaf node height. As illustrated in Fig. 2 **c**, the curvature of the 1*st* leaf is the largest, with ${x^*}_{max}$ approaching 1, and the leaf vein curvature closely resembles a symmetrical quadratic curve. In contrast, the curvatures of the 5th and 10th leaves are smaller, with ${x^*}_{max} \in (0.4, 0.7)$, and the curves are sections of the quadratic curve. To assess the accuracy of the leaf vein curvature, we calculate the leaf vein curvature angle A_{lc} (Fig. 2**a**), defined as the angle between the line connecting the leaf base and tip and the perpendicular line to the stem.

$$x_i^* = x_i/(2 \times x_{mid}) \tag{4}$$

$$z_i^* = z_i/(2 \times x_{mid}) \tag{5}$$

$$z_i^* = -arca_i \times {x_i^*}^2 + arca_i \times x_i^* (x_i^* \in [0, valuespace_i]) \tag{6}$$

$$arca_i = -0.0646 \times i^2 + 0.7276 \times i - 3.5258 \tag{7}$$

$$valuespace_i = 1.085 \times e^{(-0.0906 \times i)} \tag{8}$$

where i is the leaf order.

(e) The leaf azimuth angle refers to the orientation of the midrib centerline of each leaf in the spatial coordinate system. Maize plants have alternate leaves, and the azimuth angles of the leaves on the two sides differ by approximately 180°. Therefore, determining the azimuth angle of a single leaf is sufficient to obtain the azimuth angles of all leaves of the plant (**Eq. (9)**).

$$Azi_j = Azi_i + 180 \times (j - i), (1 \le i \le j \le N_t) \tag{9}$$

where Azi_i and Azi_j represent the azimuth angles of the leaves with sequential numbers i and j, respectively, and $Azi_i = \theta_i$ is the measured

azimuth angle of the leaf.

The mathematical description of the horizontal structure of the maize organs is based on a single stem and a single leaf. Plant-level structural parameters are also considered to obtain the horizontal structural parameters of the maize plant.

2.2.2. Mathematical description of at the plant level

Maize plants are intricate structures composed of multiple plant organs. Constructing a 3D model of a maize plant requires combining organs, such as stems and leaves, using specific rules. The structural parameters of maize plants include the maximum number of leaves on the plant, maximum height of the stem, cumulative leaf area, leaf node height, maximum width, length, and area of each leaf, and the height and diameter of each stem segment.

1) Mathematical descriptions of leaf size and leaf area.

The maize plant's cumulative leaf area (S) is closely related to the maximum number and size of leaves. The size and number of leaves are similar for a specific genotype without considering environmental factors.

a) Leaf area Ae_{max} (cm^2) of the largest leaf. The maximum number of leaves N_t denotes the maximum number of leaves on a plant during its growth period. It is primarily determined by the plant's genetic characteristics. The N_t and the minimal total leaf number (N_g) are known input parameters(Grant, 1989b). N_g denotes the minimum number of leaves under specific temperature and light cycle conditions(Grant, 1989b). The maximum length (L_{max}), minimum length (L_{max_min}), and width (W_{max}) of the largest leaf are mathematically related. This relationship is expressed in **Eq. (10)**, where k is an empirical parameter whose value was 24 cm^2 in previous studies (Grant, 1989b; Kim et al., 2012). When $N_t = N_g$, $L_{max} = L_{max_min}$. The maximum length (L_{max}) and width (W_{max}) of the largest leaf satisfy the proportional relationship in **Eq. (1)**. After obtaining L_{max} and W_{max}, the leaf area of the largest leaf on the plant (Ae_{max}) can be calculated using **Eq. (11)** (Birch et al., 1998; Fournier and Andrieu, 1998).

Initially, N_t is set to N_g, but it can be altered based on the effects of the light cycle and temperature on the final number of leaves. It depends on the plant's reproductive stage(Grant, 1989a; Kim et al., 2012). Birch et al. and Kim et al. found that Ae_{max} reached the maximum value of 1057 cm^2 when $N_t = N_g$ and $L_{max} = L_{max_min} = 115$cm. When there are differences between N_t and N_g, **Eq. (11)** can still be used to calculate the potential area Ae_{max} of the largest leaf. Muchow et al. observed that Ae_{max} reached 750 and 800 cm^2(Muchow et al., 1990) when $N_t = 18$ or 19 and Ng = 16 or 17, respectively. The leaf order N_m of the largest leaf must be calculated to describe the properties of the largest leaf on the plant. This factor is mathematically related to N_t and is expressed in **Eq. (12)**.

$$L_{max} = \sqrt{L_{max_min}^2 + k \times (N_t - N_g)} (1 \le N_g \le N_t, k = 24 cm^2) \tag{10}$$

$$Ae_{max} = L_{max} \times 0.75 \times W_{max} \times exp^{(-1.17+0.047 \times N_t)} \tag{11}$$

$$N_m = 5.93 + 0.33 \times N_t \tag{12}$$

b) Potential leaf area Ae_i(cm^2). Ae_i is defined as the surface area when the i^{th} leaf is fully expanded. It depends on the leaf sequence (i) and the maximum leaf size of the plant (Ae_{max}). The value of Ae_i is calculated using explicit equations proposed and improved by Dwyer et al., Lizaso et al., and Fournier et al. (**Eqs. (13)–(15)**. We use Ae_i to calculate the maximum length (l_{imax}) and width (w_{imax}) of the fully expanded i^{th} leaf (l_{imax} and w_{imax} satisfy the proportional relationship in **Eq. (1)**). Fig. 3**a** presents the potential leaf length, width, and area for each leaf when $N_t = 20$, Ng = 18, and$L_{max} = 115$ cm.

$$Ae_i = Ae_{max} \times \exp^{a \times \left(\frac{NL_i}{Nm} - 1\right)^2 + b \times \left(\frac{NL_i}{Nm} - 1\right)^3} \tag{13}$$

$$a = -10.61 + 0.25 \times N_t \tag{14}$$

$$b = -5.99 + 0.27 \times N_t \tag{15}$$

$$l_{imax} = \sqrt{Ae_i / [0.106 \times 0.75 \times exp^{(-1.17+0.047 \times N_t)}]} \tag{16}$$

c) Cumulative leaf area of the plant Ae_{sum}(cm^2). Ae_{sum} is the sum of the surface area of all leaves during the growth period of the maize plant; it is calculated using **Eq. (17)**. Furthermore, $GDD_{8°C}$ affects Ae_{sum}. This relationship is described in detail in the mathematical description of the maize phenological stages. The maximum value of Ae_{sum} is denoted as Ae_{sum_max}.

$$Ae_{sum} = \sum_{i=1}^{N_t} Ae_i \tag{17}$$

2) Mathematical description of leaf and stem height.

The leaf node height (h_{l_i}) is closely related to the leaf sequence (i). The h_{l_i} of the i^{th} leaf and the top height (h_i) of the stem segment where the leaf is located are considered approximately equal. Here, it is assumed that $h_{l_i} = h_i$. Previous research has shown that the height of the first leaf (h_1) remains relatively constant, with an average value of 1.5 cm(España et al., 1999). The h_i of the i^{th} leaf can be determined using **Eqs. (18)–(19)**(España et al., 1999), which consider the maximum cumulative leaf area of the plant (Ae_{sum_max}) and the maximum number of leaves (N_t). Fig. 3**b** shows the potential leaf node height for each leaf when $N_t = 20$ and $Ae_{sum_max} = 7766.5$ cm^2.

$$a_h = 3.7 - 1.10 \times N_t - 0.36 \times Ae_{sum_max} \tag{18}$$

$$h_{l_i} = h_i = \frac{(h_{N_t} - h_1)}{(N_t{}^{a_h} - 1)} \times (i^{a_h} - 1) + h_1, (1 \le i \le N_t) \tag{19}$$

where h_{N_t} represents the height of the top of the $N_t{}^{th}$ stem segment, which is affected by the $GDD_{8°C}$.

The mathematical description of individual maize plants allows for the integration of the organs, such as stems and leaves, into a static 3D model at a specific point during the growth and development. However, the 3D structure of crops is in constant flux during the growth period. The addition of crop growth equations describing the physical and chemical growth parameters over time to the static 3D maize model allows for the accurate representation of the maize plant's 3D structure during its growth period.

2.2.3. Mathematical description of maize at the season level

Yan and Hunt stated that the accurate assessment of plant temperature responses is required for establishing crop system models suitable for management(Yan and Hunt, 1999). The $GDD_{8°C}$ has been identified as an effective parameter to measure the impact of temperature on plant growth and development(McMaster and Wilhelm, 1997). In this study, we present a mathematical description of maize at the season level, specifically the effect of $GDD_{8°C}$ on maize structural parameters because $GDD_{8°C}$ provides a more accurate description of plant growth and development than the DOY. The parameters at the season level, such as the number of leaves, leaf size (leaf length, leaf width, leaf area), lifespan, stem height, and diameter, are affected by the $GDD_{8°C}$. Furthermore, maize growth occurs in three stages and at varying growth rates (initiation, development, and maturity). The growth rate is slow in the initiation stage, accelerates during the development stage, and tends to

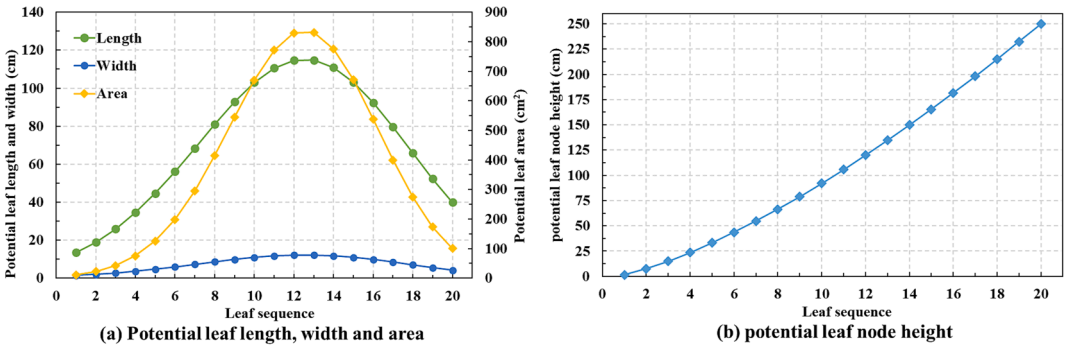


Fig. 3. Simulated leaf size and stem height at the maize plant level.

be flat during the maturity stage. We use the Pearl growth curve to describe the relationship between the $GDD_{8°C}$ and the growth and development of maize stems and leaves during leaf initiation, expansion, and senescence.

1) Mathematical description of the relationship between **$GDD_{8°C}$** and stem height and diameter.

During the three growth stages (initiation, development, and maturation), the growth rates of the maize stem (height and diameter) follow the S-shaped Pearl growth curve.

a) Pearl growth equation for stem height. The Pearl growth equation for stem height is commonly used to determine the maximum height (h_{N_t}) of maize stems. This parameter is critical for calculating the leaf node height (h_{l_i}) and the top height of the stem nodes (h_i). **Equation (20)** is established to describe the relationship between the $GDD_{8°C}$ and the maximum stem height (h_{N_t}) and maximum plant height (H_{max}) during the maize growing period. Fig. 4**a** illustrates the effect of $GDD_{8°C}$ on the simulated maximum height of the maize stem when H_{max} is 250.3 cm.

$$h_{N_t} = \frac{H_{max}}{1 + \beta \times exp^{-\alpha \times \mathrm{GDD}_{8\ ^{o}\mathrm{C}}}}, (\alpha > 0, \beta > 0) \tag{20}$$

where α and β are 0.008 and 342.1, respectively. H_{max} is the maximum stem height during the maize growing period, with an average value of 250.3 cm. The $GDD_{8°C}$ is in the range of (0, 2500) day•°C.

b) Pearl growth equation for stem diameter. The maize stem diameter ($\varnothing_{\mathrm{stem}}$) is an essential parameter for determining the aboveground biomass. **Equation (21)** is established to model the effect of $GDD_{8°C}$ on the maize stem diameter ($\varnothing_{\mathrm{stem}}$) and the maximum stem diameter ($\varnothing_{max}$) during the entire maize growth period. Fig. 4**b** depicts the simulated values; $\varnothing_{max}$=2.454 cm.

$$\varnothing_{\mathrm{stem}} = \frac{\varnothing_{max}}{1 + \delta \times exp^{-\gamma \times \mathrm{GDD}_{8\ ^{o}\mathrm{C}}}}, (\gamma > 0, \delta > 0) \tag{21}$$

where γ and δ are 0.007048 and 8.495, respectively.

2) Mathematical description of the relationship between **$GDD_{8°C}$** and the leaf growth rate during initiation, development, and senescence.

Leaf growth is a multifaceted process comprising four distinct stages: initiation, emergence, expansion, and senescence, which exhibit different growth rates. We established a Pearl growth equation describing the relationship between the $GDD_{8°C}$ and the leaf growth in these four stages.

a) Temperature-dependent growth rate function $R(T)$. $R(T)$ was first proposed by Yan and Hunt, who emphasized the importance of accurately characterizing the plant response to temperature to establish and implement accurate crop growth models(Yan and Hunt, 1999). Kim et al. subsequently improved the function using a nonlinear temperature function to measure the effect of temperature on the leaf growth rate. The improved equation (**Eq. (22)**) is as follows:

$$R(T) = R_{max} \times \frac{T_{ceil} - T}{T_{ceil} - T_{opt}} \times \left(T/T_{opt}\right)^{T_{opt}/(T_{ceil} - T_{opt})} \tag{22}$$

T is the input variable representing the average hourly environmental air temperature. T_{opt} is the optimum temperature at which leaf initiation or growth reaches its maximum rate. T_{ceil} is the highest tolerable temperature for leaf initiation and appearance. R_{max} is the maximum rate achieved during leaf initiation or growth. When $T = T_{opt}$, $R(T) = R_{max}$, and the growth and development rate reach their peak. When $T = T_{ceil}$, $R(T) = 0$, and growth and development stop.

b) Application of the temperature-dependent growth rate function $R(T)$ during leaf initiation. Leaf growth consists of four processes characterized by different development rates. Furthermore, different biological enzymes exhibit varying optimal temperatures during each developmental stage; thus, every growth phase has different optimal and maximum temperatures. The leaf tip initiation rate (R_{LTIR}) response to temperature is described by **Eq. (23)**, which sums the hourly leaf initiation rates (**Eq. (24)**). Additionally, **Eq. (25)** describes the mathematical relationship between R_{LTIR}, leaf tip appearance rate (R_{LTAR}), and $GDD_{8°C}$ (Fig. 4**c** and Fig. 4**d**).

$$R_{LTIR} = R_{\max_LTIR} \times \frac{T_{ceil_LTIR} - T}{T_{ceil_LTIR} - T_{opt_LTIR}} \times \left(T/T_{opt_LTIR}\right)^{T_{opt_LTIR}/(T_{ceil_LTIR} - T_{opt_LTIR})} \tag{23}$$

$$LTIR = \sum_{i=1}^{n} R_{LTIRi}/24 \tag{24}$$

$$GDD = \sum_{i=1}^{n} \frac{T_i - \mathrm{T}_b}{24}, (\mathrm{T}_b = 8\ ^{\circ}\mathrm{C}) \tag{25}$$

$$T_i = (T_{i_{max}} - T_{i_{min}})/2 \tag{26}$$

where T_i denotes the average hourly environmental air temperature. If T_i is not known, **Eqs. (24)–(25)** must be adjusted accordingly. R_{LTIR} represents the leaf initiation rate, and $R_{\max_LTIR}$ represents the maximum initiation rate, which is 0.978 leaves/day according to the MAIZSIM model proposed by Kim et al.(Kim et al., 2012). The optimal temperature for leaf initiation (T_{opt_LTIR}) is 30.5 °C, and the maximum tolerable temperature during leaf initiation is 42.7 °C.

c) Application of the temperature-dependent growth rate function $R(T)$ during leaf appearance. **Equation (27)** describes the relationship between the R_{LTAR} and the temperature. The hourly R_{LTAR} are summed up using **Eq. (28)** to calculate the total number of leaves. Additionally, **Eq. (25)** describes the relationship between $GDD_{8°C}$ and R_{LTAR} (Fig. 4**c** and Fig. 4**d**).

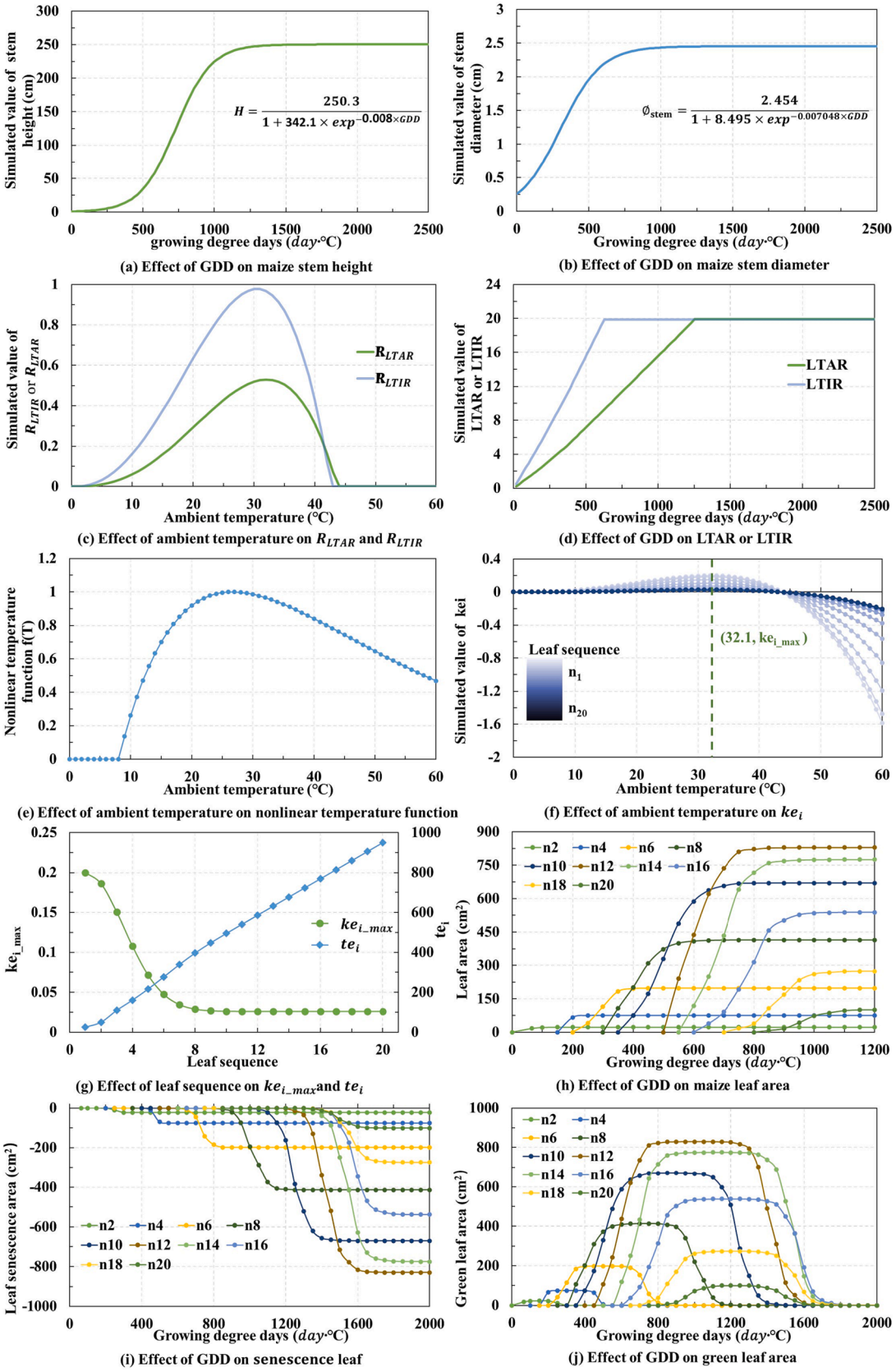


Fig. 4. Mathematical description of the relationship between $GDD_{8°C}$ and different maize leaf parameters at the season level.

$$R_{LTAR} = R_{\max_LTAR} \times \frac{T_{ceil_LTAR} - T}{T_{ceil_LTAR} - T_{opt_LTAR}} \times \left(T/T_{opt_LTAR}\right)^{T_{opt_LTAR}/(T_{ceil_LTAR} - T_{opt_LTAR})} \quad (27)$$

$$LTAR = \sum_{i=1}^{n} R_{LTARi}/24 \quad (28)$$

where T represents the average hourly environmental air temperature. R_{LTAR} denotes the leaf appearance rate, and $R_{\max_LTAR}$ is the maximum appearance rate, which is 0.53 leaves/day in this study. The optimal temperature for leaf appearance (T_{opt_LTIR}) is 32.1 °C, and the maximum tolerable temperature during leaf appearance is 43.7 °C.

d) Nonlinear temperature function $f(T)$. $f(T)$ is crucial for determining leaf growth and development. Previous studies, including those by Lisaso et al. and Fournier et al., have assumed a linear relationship between leaf growth and $GDD_{8°C}$ within a certain temperature range, although the enzyme activity decreases and cell growth and division rates slow down under high or low-temperature conditions(Fournier and Andrieu, 1998; Lizaso et al., 2003). Tollenaar et al., Bos et al., and Kim et al. employed a nonlinear temperature function to model the response more realistically(Bos et al., 2000; Kim et al., 2007; Tollenaar, 1989). Specifically, Kim et al. utilized a peak index function to measure the nonlinear leaf expansion rate in response to temperature, as shown in **Eq. (29)**(Kim et al., 2012). The function $f(T)$ calculates the maximum value. If the environmental temperature $T \le T_b = 8\,°C$, $f(T) = 0$, whereas a non-zero value is assumed when $T > T_b = 8\,°C$. Fig. 4**e** shows the effect of the ambient temperature on the response function values:

$$f(T) = \max[0, \frac{T - T_b}{T_{pk}} \times exp^{(1 - \frac{T - T_b}{T_{pk}})}] \quad (29)$$

where T_b is the base temperature used to calculate $GDD_{8°C}$, i.e., 8 °C (Kim et al., 2012). T_{pk} represents the temperature at which the potential leaf area reaches its maximum. When the environmental temperature $T = T_b + T_{pk}$, $f(T)$ reaches its maximum value of 1. Research has indicated that the peak temperature $T_{pk} = 18.7\,°C$(Fournier and Andrieu, 1998; Kim et al., 2007).

e) The dimensionless parameter ke_i is a crucial factor regulating the leaf growth rate(Lizaso et al., 2003). It is affected by the leaf order i, the total number of leaves N_t, and the environmental temperature. ke_{i_max} is the maximum expansion rate of leaf i under optimal temperature conditions; it follows a Gaussian curve. Since the leaf order $i \ge 1$ (which is the mathematical expectation of the Gaussian curve), ke_{i_max} peaks at $i = 1$, with a value of $k_o + k_x$, and then declines rapidly and levels off. **Equations (30)–(33)** are the mathematical expressions of ke_{i_max}, and Fig. 4**g** shows the effect of the leaf order i on ke_{i_max}. Fig. 4**f** illustrates the effect of the ambient temperature and leaf order on ke_i.

$$ke_{i_max} = k_o + k_x \times \exp^{(-\frac{(i-1)^2}{2W_k^2})} \quad (30)$$

$$k_x = \frac{1}{\sqrt{2\pi} W_k} \quad (31)$$

$$W_k = N_t/8.18 \quad (32)$$

$$ke_i = ke_{i_max} \times \frac{T_{cile_ke} - T}{T_{cile_ke} - T_{opt_ke}} \times (\frac{T}{T_{opt_ke}})^{T_{opt_ke}/(T_{cile_ke} - T_{opt_ke})} \quad (33)$$

where ke_{i_max} indicates the maximum rate of leaf expansion under optimal temperature conditions, k_o (=0.026) refers to the lower asymptote of the Gaussian curve, and k_x (=0.174) represents its amplitude. The variance of the Gaussian curve is denoted by W_k. The optimal temperature (T_{opt_ke}) for internal leaf growth is 18.8 °C, and the highest tolerable temperature (T_{cile_ke}) is 42.7 °C.

f) te_i and tt_i respectively indicate the $GDD_{8°C}$ when leaf i reaches 50% of its final area and the $GDD_{8°C}$ from seed emergence to the appearance of the tip of leaf i. These parameters are critical for creating a mathematical model between leaf growth and $GDD_{8°C}$ (**Eqs. (34)–(36)**(Lizaso et al., 2003). When the leaf rank $i \le 2$, te_i is a linear function of leaf rank i. In contrast, when the leaf rank $i > 2$, te_i is influenced by the leaf rank i, the total number of leaves N_t, the environmental temperature, and the nonlinear temperature function $f(T)$. The effect of the leaf rank on te_i is illustrated in Fig. 4**g**.

$$te_i = \begin{cases} 25 \times i, i \le 2 \\ tt_i + \frac{2.197}{ke_{i_max}} \times f(T), i > 2 \end{cases} \quad (34)$$

$$tt_i = (i-2) \times PHY + tt_2 \quad (35)$$

$$\mathrm{PHY} = \frac{T_{opt} - T_b}{R_{\max_LTAR}} \quad (36)$$

where PHY is the difference in the $GDD_{8°C}$ between the emergence of adjacent leaves; tt_2 is the cumulative GGDs from emergence to the growth of the second leaf. The meanings of the other parameters or variables are the same as above.

g) The leaf expansion rate R_{A_i} of the i^{th} leaf and its surface area LA_i at temperature t. The Pearl growth equation (**Eq. (38)**)(Kim et al., 2007) describes the surface area LA_i of the i^{th} leaf at temperature t, and the leaf expansion rate R_{A_i} is the first derivative of LA_i (**Eq. (37)**)(Lizaso et al., 2003). In **Eq. (38)**, the potential leaf area (Ae_i) of leaf i is the maximum value of LA_i, and when the temperature t is sufficiently high (indicating full leaf expansion), $LA_i = Ae_i$. Fig. 4**h** shows the effect of the $GDD_{8°C}$ on the LA_i for different numbers of leaves.

$$R_{A_i} = \frac{d_{A_i}}{d_t} = (Ae_i \times ke_i) \times \frac{exp^{[-ke_i \times (t - te_i)]}}{1 + exp^{[-ke_i \times (t - te_i)]}} \times f(T) \quad (37)$$

$$LA_i = \frac{Ae_i}{1 + exp^{-ke_i \times (t - te_i)}} \quad (38)$$

where t denotes the cumulative $GDD_{8°C}$ since sowing, and Ae_i is the potential leaf area obtained from **Eq. (13)**.

h) The leaf senescence rate R_{S_i} of the i^{th} leaf and its leaf area SA_i at temperature t. The Pearl growth equation is used to determine the SA_i of the i^{th} leaf at temperature t (**Eq. (40)**), and the leaf senescence rate R_{S_i} of the ith leaf is the first-order derivative of SA_i (**Eq. (39)**)(Lizaso et al., 2003). Leaf senescence is the inverse process of leaf growth. Similar to calculating the leaf expansion rate R_{A_i} and surface area LA_i of the i^{th} leaf at temperature t, the $GDD_{8°C}$ (ts_i) when 50% of the maximum area of the leaf i has senesced and the unitless parameter ks_i affecting the senescence rate are calculated. The calculation formula of ks_i and the unitless parameter ke_i controlling the growth rate are the same (**Eq. (33)**). The definition of ks_i differs from that of the $GDD_{8°C}$ when leaf i reaches 50% of its final area (te_i). The concept of the leaf lifespan LL_i is used. It is the difference between the $GDD_{8°C}$ when 50% of the maximum area of leaf i (ks_i) has senesced and the $GDD_{8°C}$ when leaf i has expanded to 50% (te_i) of its final area ($LL_i = ts_i - te_i$); it was defined in previous studies. Fig. 4**i** shows the effect of the $GDD_{8°C}$ on SA_i for different leaf orders.

$$R_{S_i} = \frac{d_{SA_i}}{d_t} = (Ae_i \times ks_i) \times \frac{exp^{[-ks_i \times (t - ts_i)]}}{1 + exp^{[-ks_i \times (t - ts_i)]}} \times f(T) \quad (39)$$

$$SA_i = \frac{-Ae_i}{1 + exp^{-ks_i \times (t - ts_i)}} \quad (40)$$

$$ts_i = LL_i + te_i \quad (41)$$

$$LL_i = L_0 + L_x * exp^{-\frac{(i - LN_L)^2}{(2 \times W_1^2)}} \quad (42)$$

$$LN_L = 3.59 + 0.498 * N_t \quad (43)$$

$$W_1 = 1/3 \times N_t \quad (44)$$

where L_0(=0) is the lower asymptote of the Gaussian curve. L_x

(=850 *day* °C) represents the amplitude of the Gaussian curve, although 500 *day* °C has been observed in some studies(Birch et al., 1998). Furthermore, LN_L denotes the node position of the leaf with the longest lifespan.

i) The green leaf area (GA_i) of the i[th] leaf at temperature t. GA_i is used to calculate the photosynthetically effective green leaf area by combining the senescent leaf area (SA_i) and the expanded leaf area (LA_i) of the ith leaf at temperature t, as defined by **Eq. (45)**. Assuming a maximum leaf count of$N_t = 20$ in maize plants, Fig. 4 **j** depicts the effect of the $GDD_{8°C}$ on the GA_i for different leaf orders. The curve has a symmetrical bell-shaped distribution, with higher values in the middle and lower values on both sides.

$$GA_i = LA_i + SA_i \tag{45}$$

2.2.4. *Mathematical description of maize at the population level*

Compared to the mathematical descriptions of maize at the organ, plant, and seasonal levels, that at the population level requires the statistical analysis of structural parameters. The population-level structural parameters include the average plant height, LAI, leaf inclination angle, within- and between-row spacing, stem zenith angle, and azimuth angle.

1) Mathematical Description of the 3D structure of the Maize Population.

It is assumed that the maize population is located on a horizontal plane, with an average plant height (H), average plant distance (d_{col}), average row distance (d_{row}), average stem zenith angle (Zen_{stem}), and average azimuth angle (Azi_{stem}). The 3D coordinates at the bottom of the maize stem's center in the i[th] column and j[th] row are expressed as (x_{ilow}, $y_{j_{low}}$,z_{low}), and those of the top in the k[th] column and l[th] row are denoted as (x_{kup},$y_{l_{up}}$,z_{up}). These coordinates are calculated using **Eqs. (46)–(48)**. Moreover, these equations can be utilized to calculate any point on the stem or leaf of the maize population.

$$x_{kup} = x_{ilow} + (k-i) \times d_{col} + \mathrm{H} \times \sin(Zen_{stem}) \times \cos(Azi_{stem}) \tag{46}$$

$$y_{l_{up}} = y_{j_{low}} + (l-j) \times d_{row} + \mathrm{H} \times \sin(Zen_{stem}) \times \sin(Azi_{stem}) \tag{47}$$

$$z_{up} = z_{low} + \mathrm{H} \times \cos(Zen_{stem}) \tag{48}$$

2) Mathematical Description of the LAI of the Maize Population.

The LAI is the ratio of the total leaf area of the plants per unit of land area. **Eq. (38)** is utilized to calculate the surface area of the i[th] leaf at temperature *t*. We assume a uniform growth. **Eq. (49)** is used to calculate the LAI of the maize population composed of α rows and β columns **Eq. (49)**.

$$LAI = (\alpha \times \beta \times \sum_{i=1}^{N_t} LA_i)/(\alpha \times d_{col} \times \beta \times d_{row}) \tag{49}$$

where N_t denotes the average maximum number of leaves.

The equations to calculate the parameters of the maize plants at the organ, individual, seasonal, and population levels combined to establish the coupled maize model, which is used to evaluate the relationship between the $GDD_{8°C}$, H_{max}, $\varnothing_{stem_max}$, d_{col}, d_{row} and N_t and the structural parameters, e.g., leaf aspect ratio, Azi_{leaf}, and leaf curvature. Fig. 5 illustrates the flowchart of the coupled maize model. Table 2 summarizes the coupled maize model's input, output, and fixed parameters.

Furthermore, to account for the variability among individual maize plants, we defined an approximate random distribution range for the main input model parameters based on statistical characteristics derived from measured data (maximum, minimum, and mean values). Specifically, a random number range of ±5 day•°C was introduced for Growing Degree Days (GDD) to capture variations during the seed germination stage. As GDD changes, differences in leaf area, leaf shape,

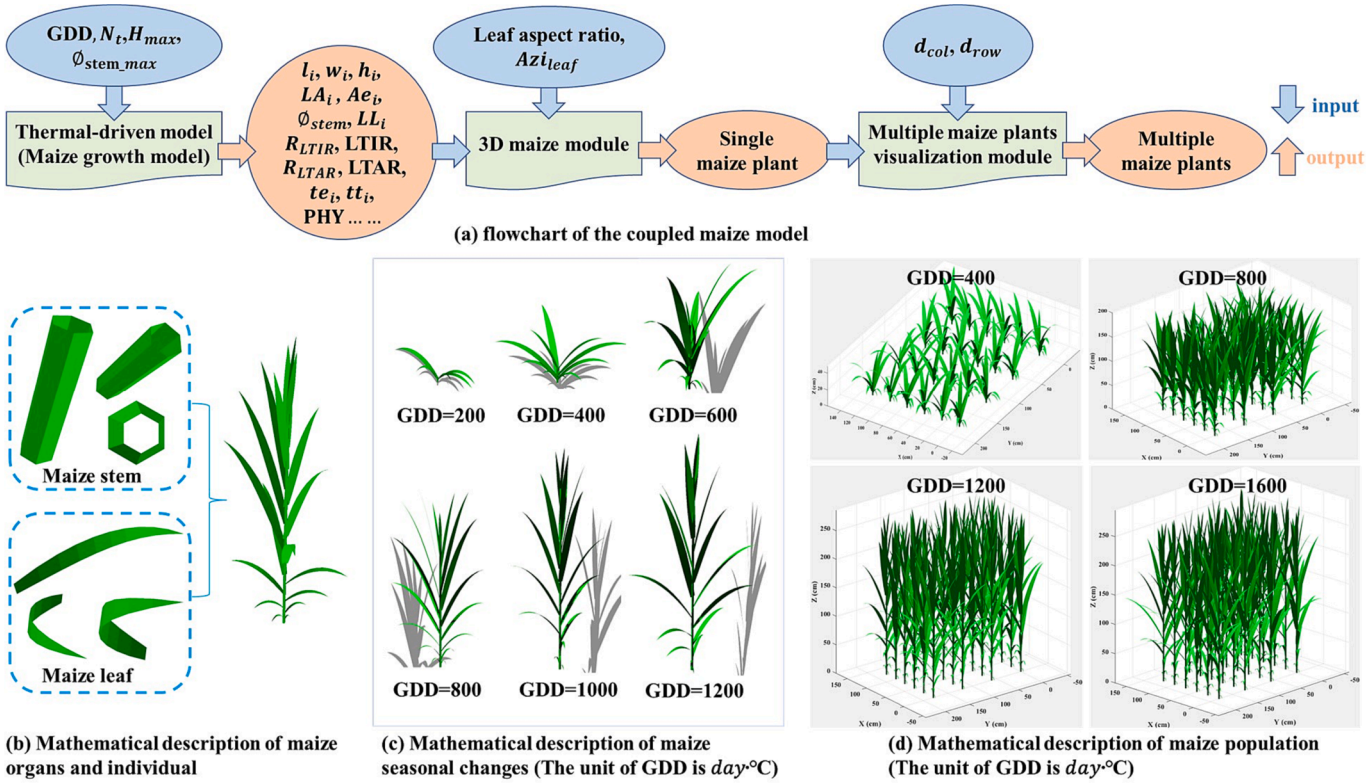


Fig. 5. Flowchart of the coupled maize model. Fig. 5a depicts the data flow among different modules of the coupled maize model and provides an overview of the key input and output variables for each module. The precise interpretations of each variable can be conveniently accessed in Table 2 by referring to their respective names or attribute information.

Table 2
Parameters of the coupled maize model. "State" indicates parameters affected by the $GDD_{8°C}$, i.e., output parameters, "Parameter" indicates fixed parameters, "Input" denotes input parameters, "Base input" denotes parameters determined by the input parameters.

Level	Name	Type	Definition	Unite
Organ level	Leaf order	Parameter	i	–
	Leaf length of the i^{th} leaf	State	l_i	cm
	Leaf width of the i^{th} leaf	State	w_i	cm
	Leaf aspect ratio	Input	LeafAspectRatio	–
	Leaf curvature	State	lc	–
	Stem diameter	State	$\varnothing_{stem}$	cm
	Leaf azimuth angle	State	Azi_{leaf}	°
Plant level	Maximum number of leaves	Input	N_t	–
	Maximum stem height	Input	H_{max}	cm
	Maximum leaf area of the plant	Input	S	cm^2
	Leaf node height of i^{th} leaf	State	h_i	cm
	Maximum leaf length	Base input	l_{imax}	cm
	Maximum leaf width	Base input	w_{imax}	cm
	Maximum leaf area	Base input	Ae_{max}	cm^2
	Maximum stem diameter	Input	$\varnothing_{stem_max}$	cm
Season level	Growing degree days	Input	$GDD_{8°C}$	$day\cdot$°C
	Temperature-dependent growth rate function	State	$R(T)$	$cm^2/(day\cdot$°C$)$
	Average hourly environmental air temperature	Base input	T_i	°C
	Maximum developmental rate for leaf initiation or growth	Parameter	R_{max}	$cm^2/(day\cdot$°C$)$
	The optimum temperature for leaf initiation or growth	Parameter	T_{opt}	°C
	The highest tolerable temperature for leaf initiation and appearance	Parameter	T_{ceil}	°C
	Leaf tip initiation rate	State	R_{LTIR}	$cm^2/(day\cdot$°C$)$
	The number of leaves being initiated	State	LTIR	–
	Maximum leaf tip initiation rate	Parameter	R_{max_LTIR}	$cm^2/(day\cdot$°C$)$
	The optimal temperature for leaf initiation	Parameter	T_{opt_LTIR}	°C
	The highest tolerable temperature for leaf initiation	Parameter	T_{ceil_LTIR}	°C
	leaf tip appearance rate	State	R_{LTAR}	$cm^2/(day\cdot$°C$)$
	The number of leaves appearing	State	LTAR	–
	Maximum leaf tip appearance rate	State	R_{max_LTAR}	$cm^2/(day\cdot$°C$)$
	The optimal temperature for leaf appearance	State	T_{opt_LTAR}	°C
	The highest tolerable temperature for leaf appearance	State	T_{ceil_LTAR}	°C
	Nonlinear temperature function	State	$f(T)$	–
	Base temperature of leaf growth and development	Parameter	T_b	°C
	The temperature at which the potential leaf area is maximized	Parameter	T_{pk}	°C
	A unitless parameter controlling the growth rate	State	ke_i	–
	The maximum rate of leaf expansion at the optimal temperature	State	ke_{i_max}	–
	The optimal temperature for leaf growth	Parameter	T_{opt_ke}	°C
	The highest tolerable temperature for leaf expansion	Parameter	T_{cile_ke}	°C
	The $GDD_{8°C}$ when leaf i reaches 50% of its final area	State	te_i	$day\cdot$°C
	The $GDD_{8°C}$ from seed emergence to the appearance of the tip of leaf i	State	tt_i	$day\cdot$°C
	The difference in the $GDD_{8°C}$ between the emergence of adjacent leaves	State	PHY	$day\cdot$°C
	The i^{th} leaf expansion rate	State	R_{A_i}	$cm^2/(day\cdot$°C$)$
	The surface area of the i^{th} leaf at temperature t	State	LA_i	cm^2
	The potential leaf area of i^{th} leaf	State	Ae_i	cm^2
	The i^{th} leaf senescence rate	State	R_{S_i}	$cm^2/(day\cdot$°C$)$
	The senesced area of the i^{th} leaf at temperature t	State	SA_i	cm^2
	A unitless parameter controlling the senescence rate	State	ks_i	–
	The $GDD_{8°C}$ when the i^{th} leaf reaches 50% of the maximum area	State	ts_i	$day\cdot$°C
	Leaf lifespan of the i^{th} leaf	State	LL_i	$day\cdot$°C
	Green leaf area of the i^{th} leaf	State	GA_i	cm^2

(*continued on next page*)

Table 2 (*continued*)

Level	Name	Type	Definition	Unite
Population-level	The average height of the plant	State	H	*cm*
	Average within-row distance	Input	d_{col}	*cm*
	Average row distance	Input	d_{row}	*cm*
	Average zenith angle of stem	State	Zen_{stem}	°
	The average azimuth angle of the stem	State	Azi_{stem}	°

and leaf insertion height manifest at the organ level. To represent variations in individual growth within the population, a random number range of ±1% H_{max} or $\varnothing_{stem_max}$ was incorporated for stem height and stem diameter. Additionally, the azimuth angle Azi_{stem} for each maize stem was randomly generated within the interval (0, 360°), and slight variations of ±1% in d_{col} or d_{row} were introduced to the ground coordinates of each maize plant. These measures ensure that each plant within the population is unique.

2.3. Evaluation metrics for assessing model accuracy

The root mean squared error (RMSE), and normalized root mean squared error (NRMSE) were used as the accuracy evaluation indices; they are defined in **Eqs. (50)–(51)**. The model fit was deemed excellent if $0.1 < \text{NRMSE}$, good if $0.1 \leq \text{NRMSE} < 0.2$, average if $0.2 \leq \text{NRMSE} < 0.3$, and poor if $\text{NRMSE} \geq 0.3$(Peng et al., 2017).

$$\text{RMSE}(ye, y) = \sqrt{\frac{1}{m}\sum_{i=1}^{m}(ye_i - y_i)^2}, i = 0, 1, \cdots, n \tag{50}$$

$$NRMSE\ ye, y = \frac{RMSE\ ye,\ y}{y^-} \tag{51}$$

where y_i, ye_i, and y^- are the measured value, predicted value, and the average of the measured maize parameter respectively.

3. Results

The differences between the output of the coupled maize model and the field measurements are attributed mainly to two factors: 1) the effect of the $GDD_{8°C}$ and 2) the systematic error resulting from the simplification of the structural parameters. The accuracy of the coupled maize model's output was quantified using field measurements of maize structural parameters, including leaf length, leaf width, leaf area, leaf node height, and plant height at six growth stages of the same variety. The $GDD_{8°C}$ values for these growth stages were 580, 680, 739, 904, 995, and 1192, respectively.

3.1. Accuracy evaluation of maize leaf size simulation

Fig. 6 and Fig. 7 show the measured and predicted maize leaf length and width, respectively in six growth periods. The predicted range of the leaf length and width for all leaf positions during the six stages were 66.429–80.178 cm and 7.905–9.228 cm, respectively. The predicted values were 9.869% and 196.637% higher than the average field

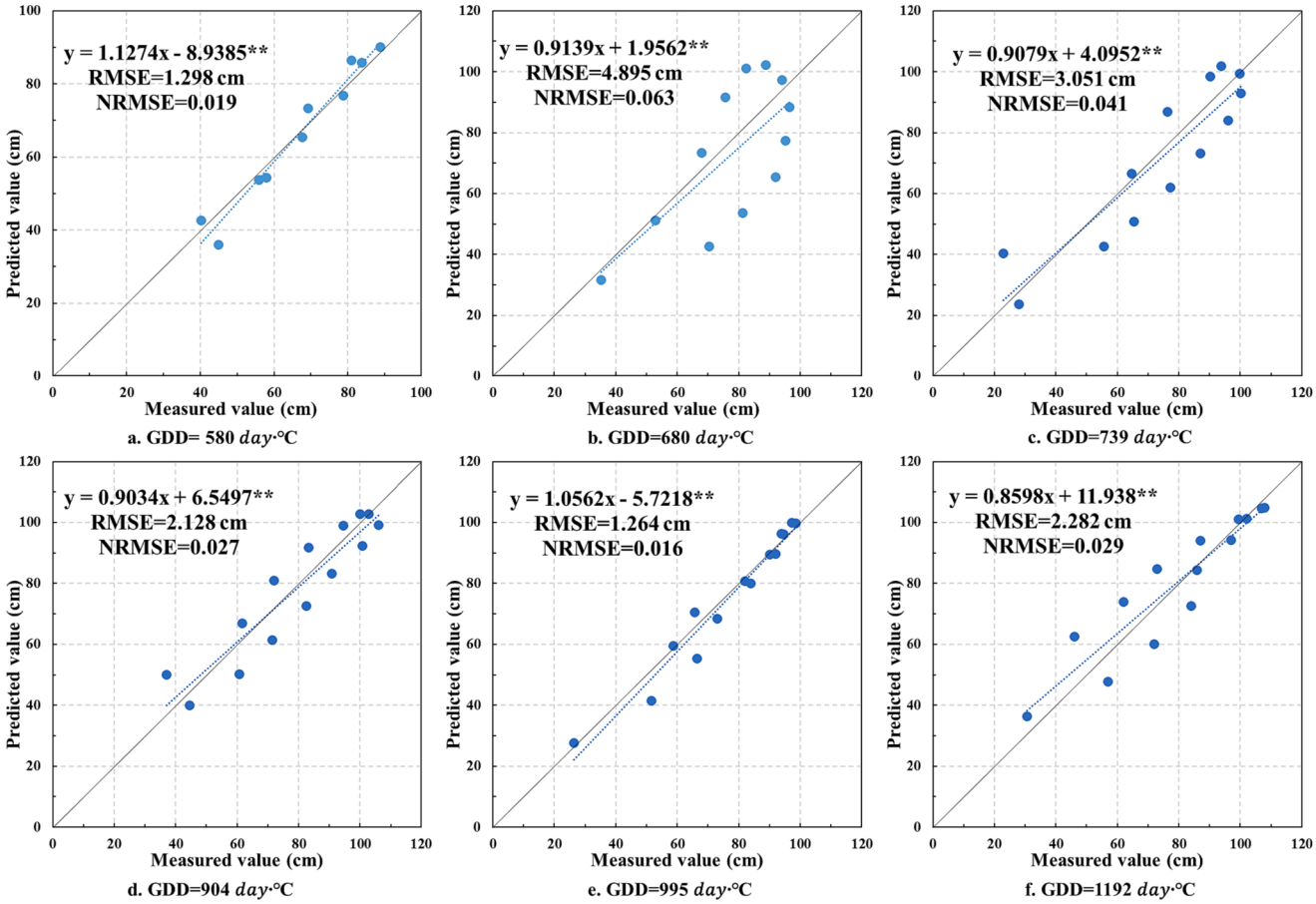


Fig. 6. Measured and predicted maize leaf length in six growth periods. The black line is the 1:1 line (*indicates statistical significance at 0.05; **indicates statistical significance at 0.01).

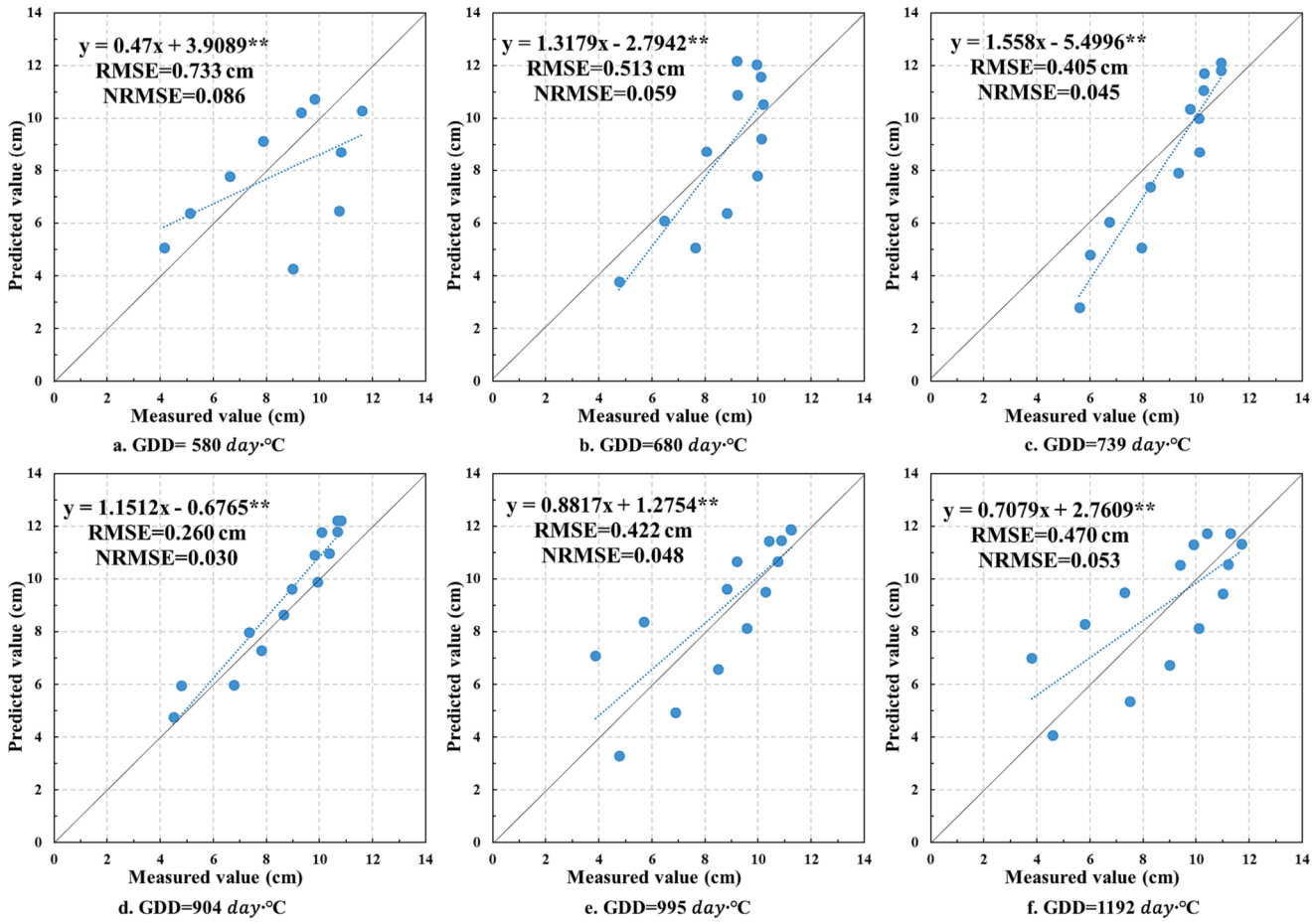


Fig. 7. Measured and predicted maize leaf width in six growth periods. The black line is the 1:1 line (*indicates statistical significance at 0.05; **indicates statistical significance at 0.01).

measurements. This difference can be attributed to the large variation in the length-to-width ratio of leaves between different plants at the same leaf position and between different leaf positions on the same plant.

Overall, the coupled maize model accurately predicts the leaf length during the six growth stages, with higher accuracy in the later stages of slow growth and development than in the middle stages of rapid growth and development. The slope of the regression equation for the measured and predicted values of maize leaf length ranges from 0.860 to 1.127 for the six stages, very close to the slope of the 1:1 line. The data points in the scatter plot are uniformly dispersed on both sides of the 1:1 line. The RMSE and NRMSE between the measured and predicted values are 1.264–4.895 cm and 0.016–0.063, respectively, indicating high prediction accuracy of the model for leaf length in the six growth stages.

Based on the slope of the fitting equation (greater than1 or less than 1), the predicted leaf lengths for the six growth periods can be classified into two categories. The first category (slope greater than 1) includes the results for GDD = 580 and 995 day•°C, (Fig. 6**a, e**). The leaf length at the intersection between the fitted line and the 1:1 line, denoted as l_{cp}, is considered the boundary. The leaf length is underestimated for leaves shorter than l_{cp} and overestimated for leaves longer than l_{cp}. For example, when GDD = 580 day•°C (Fig. 6**a**), the predicted value is lower for leaves with a length less than 70 cm and higher for leaves with a length greater than 70 cm. The second category (slope less than 1) includes the results for GDD = 680, 739, 904, and 1192 day•°C (Fig. 6**b, c, d, and f**). The predicted results are opposite to those of the first category, resulting in an overestimation of the leaf length for leaves shorter than l_{cp} and an underestimation of the leaf length for leaves longer than l_{cp}. For example, when GDD = 680 day•°C (Fig. 6**b**), the predicted value is higher for leaves with a length less than 30 cm and lower for leaves with a length greater than 30 cm. Improved prediction accuracy can only be achieved when the intersection point (l_{cp}) of the fitted line and the 1:1 line is close to the average value, and the slope is close to 1. For instance, when GDD = 680 day•°C, the measured average leaf length is 66.9 cm (Table 1), which is close tol_{cp} = 70 cm. The slope of the fitting line is 1.127, which is close to 1. Consequently, the model's prediction accuracy is significantly higher in this case.

The coupled maize model adequately predicts the leaf width in the six growth stages. However, the model's prediction accuracy for leaf width is less precise than for leaf length, and the data points are more scattered, as depicted in Fig. 7. The variability in the aspect ratio of the leaf length and width among different plants and leaf orders is the primary reason for this disparity, because the coupled maize model uses the mean value. The maize leaf shape changes significantly with the leaf node height; the lower leaves are short and slender, the middle leaves are long and wide, and the upper leaves are wide at the base and narrow rapidly toward the tip. Consequently, the leaf aspect ratio increases with the leaf order, as indicated in Table 1. The leaf aspect ratio used in the coupled maize model is the mean value (0.119) in **Eq. (1)**.

The precision of the coupled maize model in predicting leaf width depends on the accuracy of the leaf length prediction and the aspect ratio. The RMSE and NRMSE for the leaf width in Fig. 7 are 0.260–0.733 cm and 0.030–0.086, respectively, indicating high accuracy for predicting leaf width.

3.2. Accuracy evaluation of maize leaf area simulation

Unlike the leaf length and width, the leaf area is directly related to temperature-dependent parameters, such as $GDD_{8°C}$. Thus, leaf area is

more suitable for evaluating the accuracy of the coupled maize model in simulating maize structural parameters. The results indicate that the coupled maize model has high accuracy in predicting leaf area in the six growth periods. The maize leaf area predicted by the coupled maize model depends on the temperature-dependent growth rate function of the leaf area (**Eqs. (37)–(38)**, rather than the leaf length and width, which are calculated based on the leaf area and the leaf aspect ratio.

Fig. 8 shows that the slope of the regression between the measured and predicted values of the maize leaf length for the six periods ranges from 0.863 to 1.161, which is very close to the ideal slope of 1. The data points are equally distributed on both sides of the 1:1 line. The RMSE ranges from 17.950 to 42.359 cm^2, and the NRMSE for the five growth periods with GDD values of 580, 739, 904, 995, and 1192 day•°C (Fig. 8**a, c, d, e, and f**) ranges from 0.045 to 0.073, indicating high prediction accuracy. The NRMSE for the growth period with a GDD value of 680 day•°C (Fig. 8**b**) is 0.111, which is slightly larger than 0.1 but still suggests good model performance.

Fig. 8**g** depicts the effect of the $GDD_{8°C}$ on the total leaf area and growth rate of the leaf area. During the middle growth and development stage ($350 \leq GDD \leq 900$ day•°C), the leaf expansion rate $R_{A_i} \geq 5 cm^2 \cdot day^{-1} \cdot {}^{o}C^{-1}$, resulting in rapid leaf growth. Conversely, during the early or late stages of growth and development ($350\rangle$ GDD day•°C or GDD greater than 900 day•°C), the leaf expansion rate $R_{A_i} < 5 cm^2 \cdot day^{-1} \cdot {}^{o}C^{-1}$, and leaf growth is slower. Maize growth with GDD values of 580, 680, and 739 day•°C (Fig. 8**a, b, and c**) corresponds to the rapid growth stage, and GDD values of 904, 995, and 1192 day•°C (Fig. 8**d, e, and f**) represent the slow growth stage. Therefore, the coupled maize model has higher accuracy in predicting the leaf area in the last three growth periods than in the first three periods. Although the $GDD_{8°C}$ is a crucial parameter affecting maize growth, the maximum

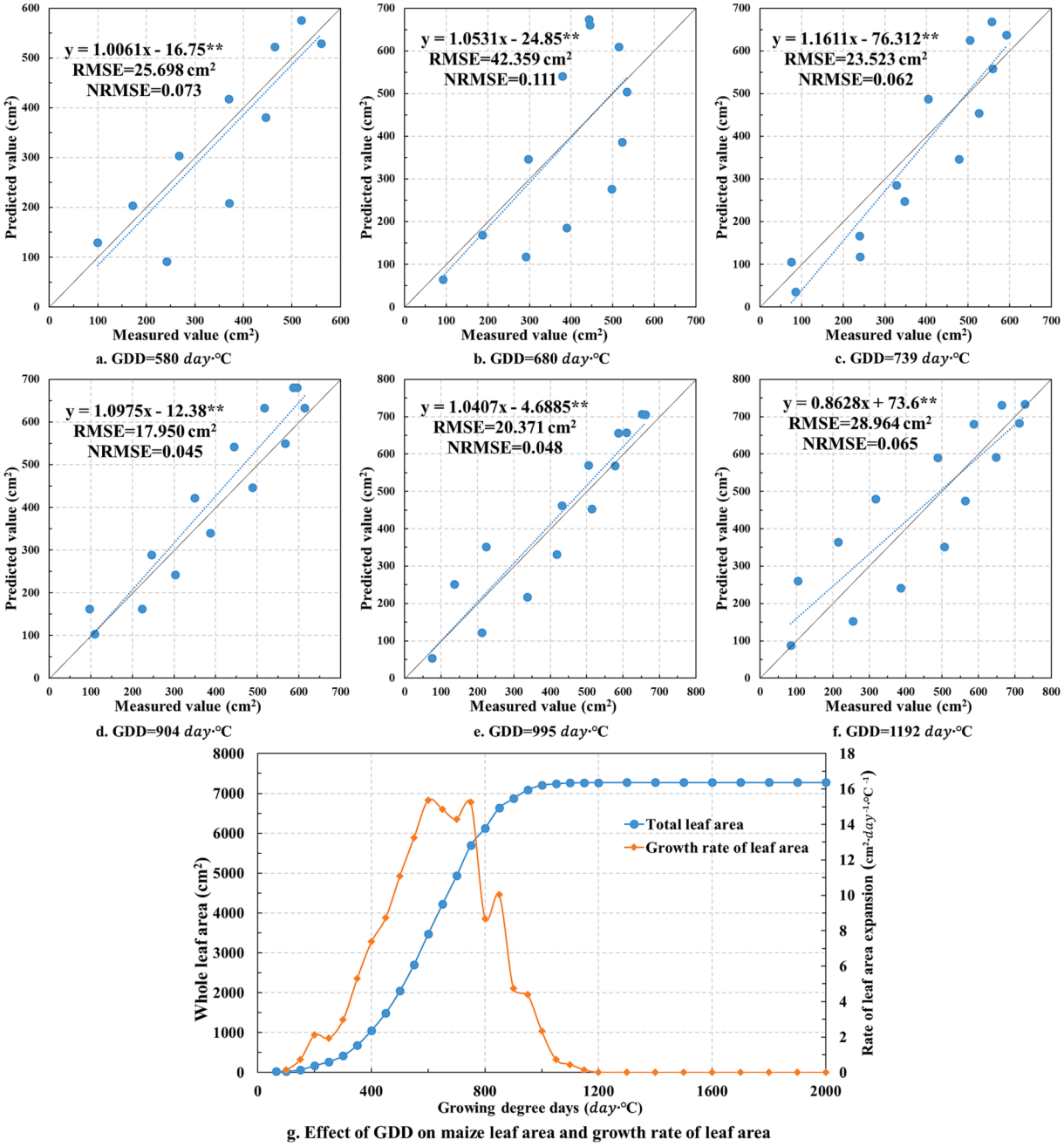


Fig. 8. Measured and predicted maize leaf area in six different growth periods (a-f). The black line is the 1:1 line. (g) Effect of GDD on leaf area (*indicates statistical significance at 0.05; **indicates statistical significance at 0.01).

number of leaves (N_t) also significantly influences the model's accuracy because it affects te_i (the $GDD_{8°C}$ from emergence to when leaf i reaches 50% of its final area, **Eq. (34)**), tt_i (the time from seed initiation to the tip of leaf i, **Eq. (35)**), and PHY (the difference in the $GDD_{8°C}$ between the emergence of adjacent leaves, **Eq. (36)**). In addition, the minimum value of the maximum leaf length (L_{max_min}) and the leaf aspect ratio also substantially affect the accuracy of leaf area prediction because of different leaf shapes.

3.3. Accuracy evaluation of maize leaf node height simulation

The coupled maize model demonstrates very high accuracy for predicting the leaf node height for the six growth periods. Similar to the leaf area prediction results, the model exhibits higher precision in the last three growth periods than in the first three growth periods. The precise prediction of the leaf node height is critical for analyzing the biophysical and biochemical parameters of different maize leaf layers and the vertical distribution of PAR.

Fig. 9 depicts the measured and predicted leaf node heights ranging from 0.960 to 1.035. The slope of the line is very close to the ideal slope of 1 for the 1:1 line, and the data points are uniformly distributed on both sides of the 1:1 line. The RMSE and NRMSE are 2.287–4.084 cm and 0.021–0.055, respectively, which are less than 0.1. These results demonstrate the excellent prediction accuracy of the coupled maize model for predicting the leaf node height in the six growth periods. Fig. 3**b** shows that the leaf node height increases with the leaf order sequence, and the slope of the line increases. This result is consistent with an increased scatter of the points with an increase in the leaf node height in Fig. 9. Moreover, Fig. 4**b** exhibits the effect of $GDD_{8°C}$ on the maize stem diameter, indicating that the leaf node height and plant height change slowly in the early and late stages of maize growth and development but rapidly in the middle stage. Therefore, the coupled maize model has higher precision in predicting the leaf node height in the last three growth periods than in the first three growth periods.

3.4. Accuracy evaluation of maize leaf curvature simulation

The coupled maize model accurately predicts the angle of leaf curvature (A_{lc}) in the six growth stages. Unlike the results for the leaf area and leaf node height, there is no clear pattern in the accuracy with the growth stage. Leaf curvature is a fundamental aspect of maize leaf morphology. Gravity significantly influences leaf curvature, resulting in a distinct parabolic curve of the leaf. We use a quadratic function to model leaf curvature, and the angle between the connecting line of the leaf base and leaf tip and the vertical line of the stem is defined as A_{lc} (refer to Fig. 2**a**). Fig. 10 shows that the regression equation slope of the measured and predicted values of A_{lc} for the six stages ranges from 0.9339 to 1.0300, which is very close to the ideal slope of 1. The data points are evenly dispersed on both sides of the 1:1 line. The RMSE ranges from 1.258 to 22.460°, and the NRMSE ranges from 0.030 to 0.046, indicating the high predictive accuracy of the coupled maize model for the leaf curvature angle for the six growth stages.

Fig. 10**g** illustrates the effect of the leaf order on the leaf curvature angle and its rate of change for GDD = 1200 day•°C andN_t = 20. A_{lc} does not increase linearly with the leaf order. The A_{lc} increases rapidly from 0 to 5 leaves, followed by slower and rapid increases up to 10 leaves. After the 10th leaf, the A_{lc} increases slowly. This pattern matches the scatterplot pattern in Fig. 10**a-f**. Although the predictive accuracy of A_{lc}

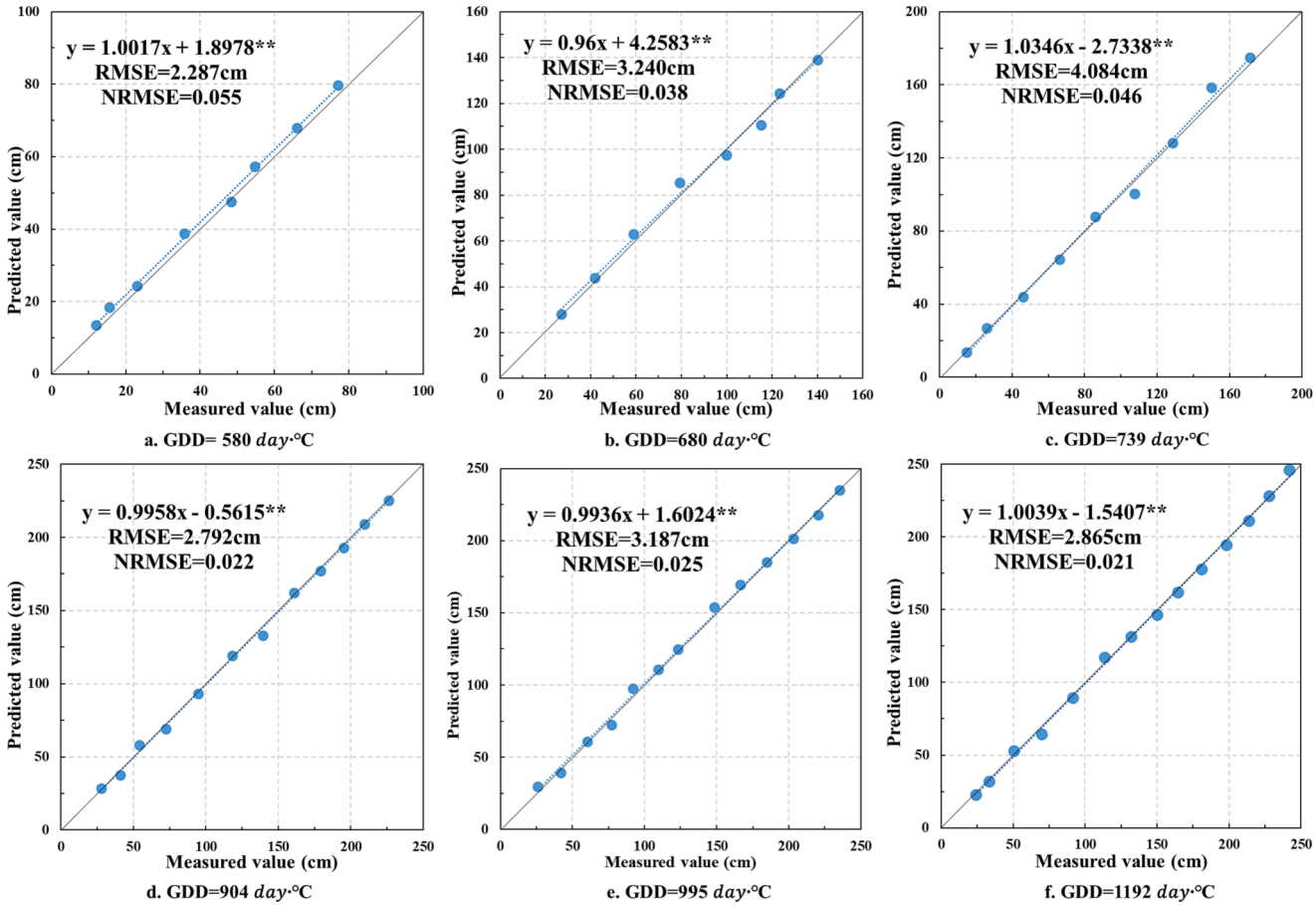


Fig. 9. Measured and predicted maize leaf node height in six growth periods. The black line is the 1:1 line (*indicates statistical significance at 0.05; **indicates statistical significance at 0.01).

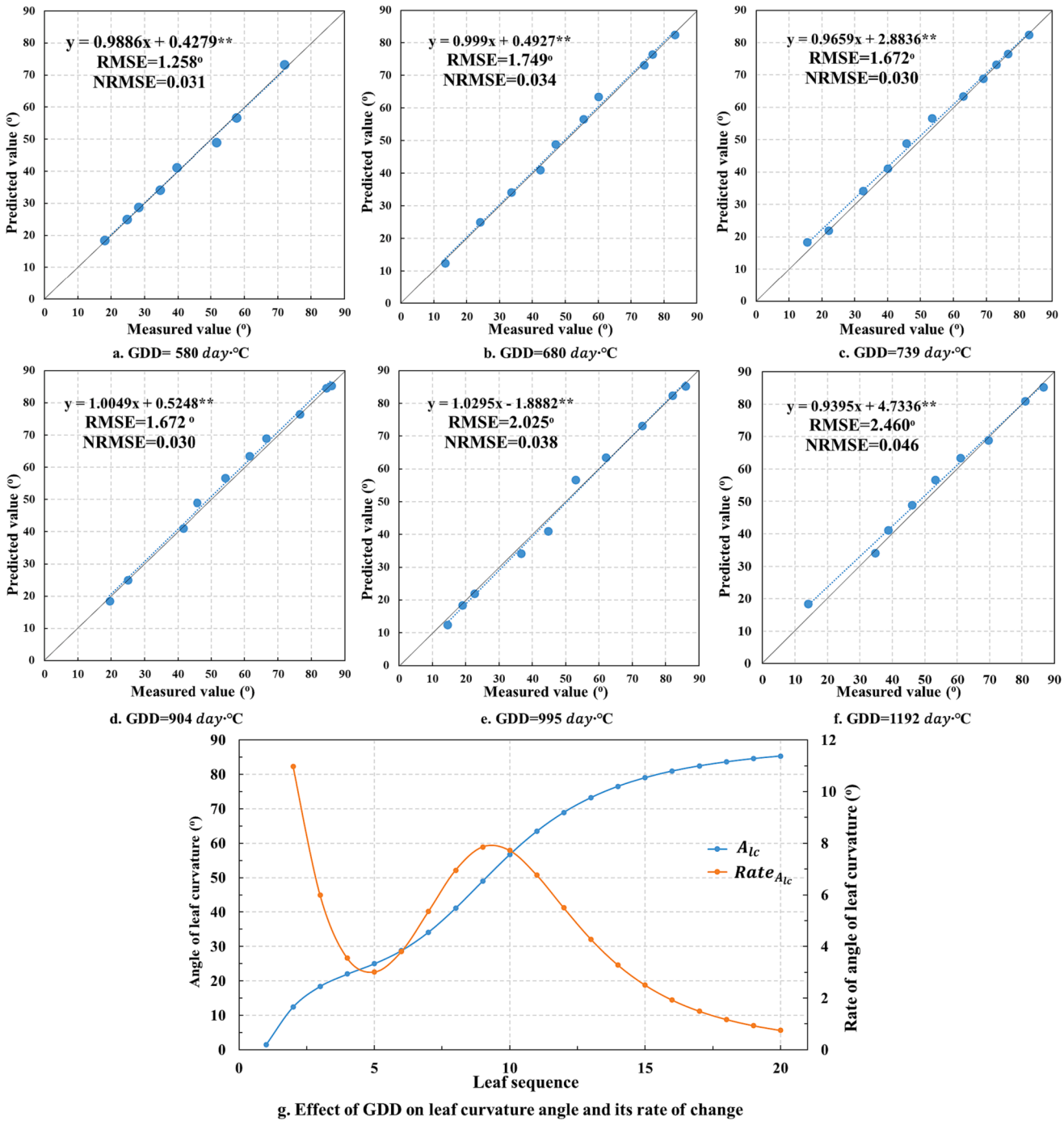


Fig. 10. Measured and predicted maize leaf curvature angle in six growth periods (a-f). The black line is the 1:1 line; g) the effect of leaf order on the leaf curvature angle and its rate of change (*indicates statistical significance at 0.05; **indicates statistical significance at 0.01).

does not seem to be related to the growth stage, A_{lc} is affected by the leaf sequence and $GDD_{8°C}$.

4. Discussion

4.1. Model suitability and accuracy

This study focuses on the structural parameters of the non-reproductive organs of maize, specifically the stem and leaves, during growth and development from germination to silking. The main objective was to address the limitations of existing crop growth models and plant functional structure models in determining the plant's responses to temperature and provide accurate dynamic simulation results and multi-scale visualizations. The suitability and accuracy of a thermal-driven crop growth model and plant functional structure algorithms for visualization were investigated. The process-based MAIZSIM model was chosen as the thermal-driven crop growth model because it has high accuracy for modeling plant responses to temperature. The MAIZSIM model characterizes maize growth using the Pearl curve, which can model plant growth characteristics accurately. Additionally, unlike other models, the thermal-driven equation of the MAIZSIM model (**Eqs. (22), 23, 27, and 29**) are exponential equations sensitive to temperature changes(Jin et al., 2016; Kim et al., 2012). Moreover, the MAIZSIM model can simulate the effect of $GDD_{8°C}$ on plant growth at the leaf or

organ level. We improved the mathematical expression of the relationship between the $GDD_{8°C}$ and the maize stem height and diameter in the MAIZSIM model. A relationship between maize stem height and leaf node height was established, and the results were verified with measured data. The RMSE between the simulated and measured values was less than 0.1, indicating high prediction accuracy (Fig. 9). The plant functional structure (3D) algorithm was simplified(España et al., 1999), and the visualization algorithm was combined with the thermal-driven crop growth model to perform a 4D reconstruction of the maize canopy at the organ and individual plant levels. The RMSEs between the simulated and measured maize leaf size (length and width), leaf area, and leaf curvature angle were less than 0.1 (in Fig. 8**b**, NRMSE = 0.11, slightly larger than 0.1), demonstrating high prediction accuracy (Fig. 6**,** Fig. 7**,** Fig. 8**,** Fig. 10). In summary, this study provides valuable insights into the structural parameters of the non-reproductive organs of maize and their relationship with $GDD_{8°C}$. The proposed models and algorithms exhibit high prediction accuracy and can improve the understanding and prediction of maize growth and development under different environmental conditions.

4.2. Model advantages and applications

This study combined thermal-driven crop growth models and plant functional structure visualization algorithms to model maize responses to temperature and provide accurate dynamic simulation results and multi-scale computer visualizations, which could not be obtained simultaneously by the two methods in the past. The coupled maize model provides simulations and computer visualizations of the maize canopy structure at the organ, plant, seasonal, and population levels. The coupled maize model's high accuracy in simulating maize canopy parameters was demonstrated through empirical data verification, indicating the model's suitability for crop growth monitoring. Additionally, the 3D models of the maize plants (".obj") can be used in remote sensing 3D radiation transfer models(Gastellu-Etchegorry et al., 2020; Qi et al., 2019), crop structure evaluations, light interception quantifications(Wen et al., 2019; Xie et al., 2017), intelligent agriculture, and for describing crop phenotypes(Li et al., 2020; Tao et al., 2022).

4.3. Model limitations and implications

The limitations of this study include limited experimental data and the experimental design, which require improvement. **First**, we reduced the number of triangular facets, ignored the wave edges of the maize leaves, and assumed a regular leaf curvature to improve the applicability of the 3D maize simulation (.obj file) in remote sensing 3D radiation transfer models and other applications (Fig. 2). This simplification resulted in differences in the leaf details between the simulated and real scenes. **Second**, we simplified the cross-sectional shape of the maize stem, assuming it was a hexagonal prism (Fig. 1), unlike the elliptical cone. **Third**, although the coupled maize model can predict the effect of $GDD_{8°C}$ on the leaf area of senescent leaves (Fig. 4**i, j**), we did not consider the senescent leaf area in the visualization of the leaves. The most crucial parameters for the visualization of the maize canopy structure (Fig. 5**a**) are the N_t and the leaf aspect ratio because they affect the empirical coefficients α, β, and γ in the leaf shape equation and are essential for the accurate 3D representation of the maize leaves (**Eq. (3)**). **Fourth**, plant population density and row spacing have great effects on maize growth, phenology and yield(Bernhard and Below, 2020; Maddonni et al., 2001), and directly affect the height and diameter of stems in the three-dimensional structure of the maize canopy. In our current model version, we have included planting density (d_{row} = 60 cm, d_{col}=25 cm), maximum plant height (H_{max}), and maximum stem diameter ($\varnothing_{stem_max}$) as three independent input parameters, while not considering the impact of population density on stem height and diameter. In future studies, we intend to conduct targeted experiments to explore this matter further. Moreover, we plan to expand the model to simulate the effects of various fertility stresses, different levels of drought, distinct stages of disease progression, and diverse plant architectures (leaf inclination distribution) on the three-dimensional structural parameters of the maize canopy.

5. Conclusion

This study proposed the coupled maize model, a 4D maize growth model consisting of a thermal-driven crop growth model (MAIZSIM) and a plant functional-structural model. The model can simulate the maize canopy at the organ, plant, seasonal, and population levels and provide multi-scale computer visualization. The coupled maize overcomes the limitations of existing crop growth models and plant functional-structural models because it simultaneously predicts maize responses to temperature and provides accurate dynamic simulation results and multi-scale computer visualizations. The experimental data confirm the model's accuracy, demonstrating its ability to provide reliable 4D representations of maize for various applications, such as remote sensing 3D radiation transfer models, crop structure assessments, light interception quantifications, smart agriculture, and crop phenotyping.

Declaration of Competing Interest

The authors declare that they have no known competing financial interests or personal relationships that could have appeared to influence the work reported in this paper.

Data availability

Data will be made available on request.

Acknowledgments

The authors would like to thank Bingrui Zhang, Shuting Qiao, Chaojia Nie, Rui Hou, Fu Wen, and Wei Peng for collecting the field measurement data at Beijing Tongzhou District.

Author Contributions

B.Q. designed the research, performed data analysis, and wrote the manuscript. W.H. and A.G. guided the research. D.X. guided the key procedures for 3D maize modeling. H.Y., Q.X., and Q.J. assisted in reviewing and editing the manuscript. Y.J. participated in translating the paper. Y.P. and C.R. provided suggestions for the study. T.X., Y.Z. and T.N provided experimental guidance and meteorological data. All authors have read and approved the final version of the manuscript for publication.

Funding

This research was funded by the National Key R&D Program of China [grant numbers 2021YFB3900501]; National Natural Science Foundation of China [grant numbers 42071330, 42201365]; Hainan Provincial Natural Science Foundation of China [grant numbers 322QN346, 422QN349]; Hainan Province Science and Technology Special Fund [grant numbers ZDYF2021GXJS038]; SINO- EU, Dragon 5 proposal: Application Of Sino-Eu Optical Data Into Agronomic Models To Predict Crop Performance And To Monitor And Forecast Crop Pests And Diseases [grant numbers 57457]; Global Crop Pest and Disease Habitat Monitoring and Risk Forecasting(CROP PEST MONITORING).

References

Allen, M., Prusinkiewicz, P., DeJong, T., 2005. Using L-systems for modeling source–sink interactions, architecture and physiology of growing trees: the L-PEACH model. New Phytol. 166, 869–880.

Bernhard, B.J., Below, F.E., 2020. Plant population and row spacing effects on corn: Plant growth, phenology, and grain yield. Agron. J. 112, 2456–2465.

Birch, C., Hammer, G., Rickert, K., 1998. Improved methods for predicting individual leaf area and leaf senescence in maize (Zea mays). Aust. J. Agr. Res. 49, 249–262.

Bos, H., Tijani-Eniola, H., Struik, P., 2000. Morphological analysis of leaf growth of maize: responses to temperature and light intensity. NJAS: Wageningen Journal of. Life Sci. 48, 181–198.

de Reffye, P., Hu, B., Kang, M., Letort, V., Jaeger, M., 2020. Two decades of research with the GreenLab model in agronomy. Ann. Bot. 127, 281–295.

España, M.a.L., Baret, F., Aries, F., Chelle, M., Andrieu, B., Prévot, L., 1999. Modeling maize canopy 3D architecture: Application to reflectance simulation. Ecological Modelling 122, 25-43.

Fournier, C., Andrieu, B., 1998. A 3D architectural and process-based model of maize development. Ann. Bot. 81, 233–250.

Gao, F., Anderson, M.C., Zhang, X., Yang, Z., Alfieri, J.G., Kustas, W.P., Mueller, R., Johnson, D.M., Prueger, J.H., 2017. Toward mapping crop progress at field scales through fusion of Landsat and MODIS imagery. Remote Sens. Environ. 188, 9–25.

Gastellu-Etchegorry, J.-P., Wang, Y., Regaieg, O., Yin, T., Malenovsky, Z., Zhen, Z., Yang, X., Tao, Z., Landier, L., Al Bitar, A., 2020. Recent Improvements in the Dart Model for Atmosphere, Topography, Large Landscape, Chlorophyll Fluorescence, Satellite Image Inversion, IGARSS 2020–2020 IEEE International Geoscience and Remote Sensing Symposium. IEEE 3455–3458.

Grant, R., 1989a. Simulation of carbon assimilation and partitioning in maize. Agron. J. 81, 563–571.

Grant, R., 1989b. Simulation of maize phenology. Agron. J. 81, 451–457.

Griffon, S., De Coligny, F., 2014. AMAPstudio: an editing and simulation software suite for plants architecture modelling. Ecol. Model. 290, 3–10.

Hemmerling, R., Evers, J.B., Smoleňová, K., Buck-Sorlin, G., Kurth, W., 2013. Extension of the GroIMP modelling platform to allow easy specification of differential equations describing biological processes within plant models. Comput. Electron. Agric. 92, 1–8.

Jin, Z., Zhuang, Q., Tan, Z., Dukes, J.S., Zheng, B., Melillo, J.M., 2016. Do maize models capture the impacts of heat and drought stresses on yield? Using algorithm ensembles to identify successful approaches. Glob. Chang. Biol. 22, 3112–3126.

Kim, S.-H., Gitz, D.C., Sicher, R.C., Baker, J.T., Timlin, D.J., Reddy, V.R., 2007. Temperature dependence of growth, development, and photosynthesis in maize under elevated CO2. Environ. Exp. Bot. 61, 224–236.

Kim, S.H., Yang, Y., Timlin, D.J., Fleisher, D.H., Dathe, A., Reddy, V.R., Staver, K., 2012. Modeling temperature responses of leaf growth, development, and biomass in maize with MAIZSIM. Agron. J. 104, 1523–1537.

Li, Z., Guo, R., Li, M., Chen, Y., Li, G., 2020. A review of computer vision technologies for plant phenotyping. Comput. Electron. Agric. 176, 105672.

Li, B., Ma, M., Chen, S., Li, X., Chen, S., Zheng, X., 2022. Temporal Variation and Component Allocation Characteristics of Geometric and Physical Parameters of Maize Canopy for the Entire Growing Season. Remote Sens. (Basel) 14, 3017.

Lizaso, J.I., Batchelor, W.D., Westgate, M.E., 2003. A leaf area model to simulate cultivar-specific expansion and senescence of maize leaves. Field Crop Res 80, 1–17.

Maddonni, G., Otegui, M.E., Cirilo, A.G., 2001. Plant population density, row spacing and hybrid effects on maize canopy architecture and light attenuation. Field Crop Res 71, 183–193.

McMaster, G.S., Wilhelm, W.W., 1997. Growing degree-days: one equation, two interpretations. Agric. For. Meteorol. 87, 291–300.

Muchow, R.C., Sinclair, T.R., Bennett, J.M., 1990. Temperature and solar radiation effects on potential maize yield across locations. Agron. J. 82, 338–343.

Peng, J.-L., Kim, M.-J., Jo, M.-H., Min, D.-H., Kim, K.-D., Lee, B.-H., Kim, B.-W., Sung, K.-I., 2017. Accuracy evaluation of the crop-weather yield predictive models of Italian ryegrass and forage rye using cross-validation. J. Crop Sci. Biotechnol. 20, 327–334.

Qi, J., Xie, D., Yin, T., Yan, G., Gastellu-Etchegorry, J.-P., Li, L., Zhang, W., Mu, X., Norford, L.K., 2019. LESS: LargE-Scale remote sensing data and image simulation framework over heterogeneous 3D scenes. Remote Sens. Environ. 221, 695–706.

Tao, H., Xu, S., Tian, Y., Li, Z., Ge, Y., Zhang, J., Wang, Y., Zhou, G., Deng, X., Zhang, Z., 2022. Proximal and remote sensing in plant phenomics: Twenty years of progress, challenges and perspectives. Plant. Communications 100344.

Tardieu, F., Cabrera-Bosquet, L., Pridmore, T., Bennett, M., 2017. Plant phenomics, from sensors to knowledge. Curr. Biol. 27, R770–R783.

Tollenaar, M., 1989. Response of dry matter accumulation in maize to temperature: I. Dry matter partitioning. Crop Science 29, 1239–1246.

Vos, J., Evers, J.B., Buck-Sorlin, G.H., Andrieu, B., Chelle, M., De Visser, P.H., 2010. Functional–structural plant modelling: a new versatile tool in crop science. J. Exp. Bot. 61, 2101–2115.

Wang, N., Wang, E., Wang, J., Zhang, J., Zheng, B., Huang, Y., Tan, M., 2018. Modelling maize phenology, biomass growth and yield under contrasting temperature conditions. Agric. For. Meteorol. 250, 319–329.

Wen, W., Guo, X., Li, B., Wang, C., Wang, Y., Yu, Z., Wu, S., Fan, J., Gu, S., Lu, X., 2019. Estimating canopy gap fraction and diffuse light interception in 3D maize canopy using hierarchical hemispheres. Agric. For. Meteorol. 276, 107594.

Wu, M., Zhu, Q., Wang, J., 2002. Structural parameter calculation of summer maize and visualization of maize canopy in field. Acta Agron. Sin. 28, 721–726 in Chinese with English abstract.

Xie, D., Qin, W., Wang, P., Shuai, Y., Zhou, Y., Zhu, Q., 2017. Influences of Leaf-Specular Reflection on Canopy BRF Characteristics: A Case Study of Real Maize Canopies With a 3-D Scene BRDF Model. IEEE Trans. Geosci. Remote Sens. 55, 619–631.

Yan, W., Hunt, L., 1999. An equation for modelling the temperature response of plants using only the cardinal temperatures. Ann. Bot. 84, 607–614.